AMERICAN MUSEUM NOVITATES

Number 3986, 36 pp. February 16, 2022

New diminutive Eocene lizard reveals high K-Pg survivorship and taxonomic diversity of stem xenosaurs in North America

KRISTER T. SMITH,[1] BHART-ANJAN S. BHULLAR,[2] AND JONATHAN I. BLOCH[3]

ABSTRACT

We describe a new diminutive early Eocene lizard, *Blutwurstia oliviae*, gen. et sp. nov., on the basis of associated cranial and postcranial remains from the Clarks Fork Basin of Wyoming. Results from phylogenetic analyses suggest that *B. oliviae* is on the stem of knob-scaled lizards (*Xenosaurus*), a relict extant clade of specialized, stenotopic crevice-dwellers from Mexico and Central America. Results further suggest that *B. oliviae* is basal to all other previously described pan-xenosaurs (members of Pan-Xenosaurus, the total clade of *Xenosaurus*) except species of *Entomophontes*, to which it is closely related. Given that *B. oliviae* and *Entomophontes* are known from a limited fossil record, with only one recovered element (the maxilla) in common, the level of support for this relationship is surprisingly high. We use a posteriori time-calibrated trees and ghost lineages (maximum parsimony) and divergence time estimates under the fossilized birth-death process (Bayesian inference) to infer patterns of extinction across the Cretaceous-Paleogene (K-Pg) boundary in Pan-Xenosaurus, including those consistent with pseudoextinction. Whereas the fossil record documents a single lineage in the latest Cretaceous, results from analyses using these analytical methods suggest that three or more species existed, with high survivorship across the K-Pg boundary. The surviving

[1] Department of Messel Research and Mammalogy, Senckenberg Research Institute, and Faculty of Biological Sciences, Institute for Ecology, Diversity and Evolution, Goethe University Frankfurt, Frankfurt am Main, Germany.

[2] Department of Earth and Planetary Sciences and Peabody Museum of Natural History, Yale University, New Haven, Connecticut; and Division of Paleontology, American Museum of Natural History, New York, New York.

[3] Florida Museum of Natural History, University of Florida, Gainesville, Florida.

 ISSN 0003-0082

lineages were apparently present at proximal to intermediate distance from the Chicxulub impact site, thought to have a causal relationship with extinctions across the K-Pg boundary. The premaxilla and dorsal vertebrae of *E. incrustatus* and *B. oliviae*, respectively, independently suggest that each of these taxa had a depressed body form consistent with extant crevice-dwelling squamates, which may have played a role in the high survivorship of pan-xenosaur lineages across the K-Pg boundary.

INTRODUCTION

The anguimorph lizard total clade Pan-Xenosaurus (Smith and Gauthier, 2013) includes the extant taxon *Xenosaurus* (knob-scaled lizards) and a number of extinct stem lineages (Gauthier, 1982; Estes, 1983; Bhullar, 2011; Smith and Gauthier, 2013). Genetic evidence strongly supports the hypothesis that *Xenosaurus* belongs to a clade, Neoanguimorpha, that also includes *Heloderma* (gila monsters and beaded lizards) and Anguidae (alligator lizards, glass lizards, galliwasps, etc.) (Fry et al., 2006; Hedges and Vidal, 2009; Vidal et al., 2012; Pyron et al., 2013; Reeder et al., 2015; Zheng and Wiens, 2016; Burbrink et al., 2020). There is little morphological support for this proposed clade (Gauthier et al., 2012), although a few characters have been cited as possible synapomorphies (Čerňanský et al., 2014). One extant (Anguinae) and one extinct (Glytposaurinae) lineage of Anguidae as well as a stem relative of *Heloderma* are inferred to have dispersed to the Old World from North America (Smith, 2009).

All three proposed lineages of Neoanguimorpha existed at the time of the Chicxulub bolide impact (Alvarez et al., 1980) that corresponds with the Cretaceous-Paleogene (K-Pg) boundary. The oldest documented stem member of the *Heloderma* lineage, *Primaderma nessovi*, was recovered from 98.4 Ma strata of the Cedar Mountain Formation in Utah (Nydam, 2000). We note that results from some recent phylogenetic analyses using combined evidence suggest that proposed Cretaceous relatives of *Heloderma* from Asia are more closely related to monitor lizards, Varanidae (Reeder et al., 2015), whereas others (Conrad et al., 2011; Yi and Norell, 2013) have supported the more traditional topology (Norell and Gao, 1997). Probable stem xenosaurs are known from the early Campanian of Canada (Gao and Fox, 1996), as are the earliest (stem?) members of Anguidae (Gao and Fox, 1996).

More specifically, all three proposed lineages of Neoanguimorpha are known from Rocky Mountain interior of North America up to the K-Pg boundary. The total clades of *Heloderma*, Anguidae, and *Xenosaurus* are documented in the latest Cretaceous of Wyoming and Montana by *Paraderma bogerti*, *Odaxosaurus piger*, and *Exostinus lancensis*, respectively (Estes, 1964; Gao and Fox, 1996). The proximity of squamates (lizards and snakes) in the Western Interior of North America to the Chicxulub impact site may have contributed to a severe reduction in overall species diversity (Longrich et al., 2012), particularly among conspicuous groups of "scincomorphs" (MacLeod et al., 1997; Nydam, 2013).

A single lineage of pan-xenosaurs is documented at the end of the Cretaceous and in the earliest Paleocene (Longrich et al., 2012). In other words, while species diversity may have been low around the K-Pg boundary, no extinction is recorded across it. Phylogenetic tree topologies are not always congruent with the stratigraphic pattern of fossil occurrences, implying "ghost

lineages" not yet recorded by direct fossil evidence (e.g., Norell, 1992; Smith, 1994). Assuming these topologies are a true representation of relationships can thus influence the interpretation of taxonomic diversity patterns through time. Furthermore, a nonbifurcating lineage may become so substantially transformed from one time slice to the next that it is recognized as a different taxonomic species, whereby the nominal ancestral species disappears, a phenomenon called pseudoextinction (e.g., Archibald, 1993). In this paper, we describe a new diminutive species of lizard from the early Eocene of Wyoming. Based on the results of phylogenetic analyses, which suggest it is on the stem of *Xenosaurus*, and its inferred paleoecology, we then examine broader survivorship patterns among stem xenosaurs across the K-Pg boundary.

MATERIALS AND METHODS

Geologic Setting and Age

The holotype and only known specimen of the new taxon (USNM PAL 768729) consists of associated elements that were recovered from freshwater limestone collected near University of Michigan fossil locality SC-4, the 8abc limestone (fig. 1; see Beard and Houde, 1989; Bloch and Bowen, 2001; Bloch and Boyer, 2001; Bowen and Bloch, 2002). The fossil bed is early Eocene in age (Wa-1 faunal zone of the Wasatchian North American Land Mammal Age; 1570 m above the K-Pg boundary), in the Willwood Formation, Clarks Fork Basin, Park County, Wyoming. Detailed locality information is archived at the University of Michigan Museum of Paleontology (see also Gingerich, 2001). We take its age to be 56–55 Ma.

Size

To estimate snout-vent length (SVL), we created a dataset of tooth height (measured in the middle of the maxilla) and SVL for iguanid lizards (appendix). Although the taxon sampling might not be ideal, the clade Iguanidae (= Pleurodonta) is close to Anguimorpha in molecular phylogenies, neither Iguanidae nor *Xenosaurus* shows a marked propensity to lengthening of the teeth, and insufficient measurable specimens of Anguimorpha were available. Moreover, owing to the paucity of small anguimorph species, extrapolation would have been necessary. Because taxa classified as *Xenosaurus* generally have more vertebrae than typical iguanids (Gauthier et al., 2012), our estimates of SVL for USNM PAL 768729 and other stem xenosaurs are likely to be slight underestimates. We ln-transformed the data, regressed ln(SVL) on ln(tooth height), estimated ln(SVL) and 95% confidence interval on the slope, and then back-transformed ln(SVL) to obtain SVL.

Phylogenetic Analyses

Maximum parsimony: To infer the phylogenetic relationships of the new taxon, we coded morphology of the holotype using the 274-character data matrix of Bhullar (2011), which, while focused on xenosaurs, includes representatives of all major anguimorph lineages. We excluded *Carusia intermedia*, as this species has recently been determined to be a stem scincid (Gauthier et al., 2012; Reeder et al., 2015) as well as the fossil helodermatids *Eurheloderma*

gallicum and *Primaderma nessovi*. The iguanid *Pristidactylus torquatus* was used as the outgroup. Thus, the modified dataset included 24 species. We added the following new characters [appended to the end of the Bhullar (2011) matrix so character numbers are unchanged]:

275. Tooth shafts in cross section just above jaw parapet: (0) rounded, (1) with strong mesial and distal carinae.
276. Teeth, lingual surface: (0) curvature smooth in horizontal section, (1) pair of longitudinal grooves interrupts curvature (*Entomophontes hutchisoni* only).
277. Teeth, anterior teeth (0) same height as teeth in middle of jaw, (1) much lower-crowned than teeth in middle of jaw.
278. Frontal scute: (0) large and azygous, spanning the entire interorbital width of the frontal bone, (1) fragmented, not identifiable.
279. Frontoparietal scute: (0) large and paired, touching one another on the midline, (1) fragmented, not identifiable.
280. Parietal scute: (0) large and paired, extending significantly posterior to the posterior margin of the interparietal scute, (1) partially or wholly fragmented.

Of the 280 characters, 256 are parsimony informative. The modified matrix was analyzed (1a) without any topological constraint using maximum parsimony (MP) in PAUP* v.4.0a release 161 (https://paup.phylosolutions.com) with the following settings: heuristic search, random addition sequence, 1000 repetitions, TBR branch-swapping. Because molecular data strongly support a different topology of anguimorph phylogeny than the morphological one (e.g., Fry et al., 2006; Pyron et al., 2013), we conducted a second analysis (1b) in which a minimum basic outline of the molecular tree (Reeder et al., 2015) was enforced as a backbone: (((*Heloderma suspectum* (*Elgaria multicarinata, Xenosaurus grandis*)), (*Shinisaurus crocodilurus* (*Lanthanotus borneensis, Varanus exanthematicus*))). In each analysis, clade support was assessed using 1000 bootstrap pseudoreplicates, each with the same settings given previously.

A posteriori time scaling: The single MP tree was time-scaled a posteriori using the three-parameter calibration model of Bapst (2013). The three rate priors (speciation, extinction, fossilization) were taken as the median parameter estimates from the results of the Bayesian inference analyses (see below) using the fossilized birth-death model with sampled ancestors. The stratigraphic ranges of fossil taxa other than the new taxon represented by USNM PAL 768729 (see above) are as follows:

The oldest documented specimens of *Exostinus lancensis* are from the Lancian (Gao and Fox, 1996). Sahni (1972) reported a maxilla of this species in the Judithian, probably the occurrence to which Bryant (1989) and Archibald and Bryant (1990) referred; the single specimen was reported to be indistinguishable from *E. lancensis* but also to lack accessory cusps (Sahni, 1972), and Gao and Fox (1996) noted other differences between Sahni's material and *Ex. lancensis*. We conservatively take the lower age limit of the species range to be the base of chron C31n (Cifelli et al., 2004). In the early Paleocene, the species is also reported from the Puercan (Archibald and Bryant, 1990; Longrich et al., 2012). It is furthermore

reported from one Torrejonian assemblage each in Montana (Estes, 1976) and (tentatively) in Wyoming (Sullivan, 1982). The former is correlated with the Rock Bench fauna (Jepsen in Estes, 1976; Bartels, 1987). Conservatively we take the top of chron C27n to be the upper limit on its age. The chronologic range of *Ex. lancensis* is thus 69.3–62.2 Ma.

The type specimen of *Restes rugosus* (Gilmore, 1942) comes from Princeton Quarry at Polecat Bench, Wyoming, assigned to Tiffanian zone Ti-5a (Secord, 2008). The base of Ti-5a is just above the top of C26n (Secord et al., 2006), which is taken as a conservative lower limit on the known range. Other specimens are described from locality SC-188 (Bartels, 1987), assigned to Clarkforkian zone Cf-2. Wasatchian-aged specimens previously assigned to *R. rugosus* have been reinterpreted as belonging to a stem-shinisaur (Smith and Gauthier, 2013). Caldwell (2003) noted that the snout tip affixed to Bridgerian-age *Saniwa ensidens* USNM PAL 2185 belongs to a different species, which he identified as cf. *Restes* sp.; our study of the specimen indicates that the snout tip probably pertains to the Eocene iguanid genus *Parasauromalus*, based on overall similarity and the highly unusual and apomorphic overlap of the premaxilla on the maxilla, a character otherwise almost exclusively seen in the extant genus *Polychrus* and its stem (Smith, 2006, 2011). A conservative upper limit on the known range of the species is therefore the Paleocene-Eocene boundary. The chronologic range of *R. rugosus* is thus 59.0–56.0 Ma.

The oldest known specimens of *Entomophontes incrustatus* are from the main phase of the carbon isotope excursion of the Willwood Formation in the Bighorn Basin, Wyoming (Yans et al., 2006; Smith, 2009), in Wasatchian zone Wa-0. The base of the CIE, which lasted around 180 Kyr, marks the Paleocene-Eocene boundary (Dupuis et al., 2003). A conservative lower limit on the distribution of the species is taken to be the Paleocene-Eocene boundary. The latest occurrences are as high as the Lysitean, or Wasatchian zone Wa-6 (Smith and Gauthier, 2013). According to Wing et al. (1991), the top of the Lysitean lies below the Ar-Ar-dated tuff at 52.8 Ma. The chronologic range of *En. incrustatus* is thus 56.0–52.8 Ma. Note that "*Entomophontes incrustatus*" was reported from Cf-3 by Bartels (1987, table 9), but that work did not make the name available (at the time, a nomen nudum). The specimens on which this identification was based have not been published and thus not confirmed; this record is not taken into account here.

The oldest specimens of *Entomophontes hutchisoni* are from Dorsey Creek Quarry in Wasatchian zone Wa-5 (Smith, 2011; Smith and Gauthier, 2013). In the Bighorn Basin the base of Wa-5 is marked by the first appearance of *Bunophorus etsagicus*, which is around the base of C24n (Flynn and Tauxe, 1998; Smith, 2001). The latest occurrences are from Tabernacle Butte in Bridgerian zone Br-3 (Smith and Gauthier, 2013). According to McCarroll et al. (1996), the top of the Adobe Town Member and zone Br-3 lie in chron C21n, whose upper limit is taken as a conservative age for the top of the range of this species. The chronologic range of *En. hutchisoni* is thus 54.0–45.7 Ma.

Specimens of *Exostinus serratus* that were explicitly studied phylogenetically (Bhullar, 2010, 2011) are: AMNH 1608 (holotype), AMNH 7726, and USNM v16565. The former two are historical material described by Cope (1873) from Logan Co., Colorado. An Orellan age

can be assumed (Estes, 1983), but nothing more precise. The last specimen was collected in 1931 from the Brule Formation of Converse Co., Wyoming, and is also Orellan in age. The base of the Orellan is taken to be coincident with the Eocene-Oligocene boundary (Prothero and Swisher, 1992). The top of the Orellan falls in magnetochron C12r (Prothero and Emry, 2004), but three Ar-Ar dates (different minerals) from the lower Whitneyan average 31.8 Ma, which we take as a conservative upper limit on its range. The chronologic range of *Ex. serratus* is thus 33.9–31.8 Ma.

The age range of *Exostinus serratus* describes uncertainty in its stratigraphic distribution, whereas the age ranges of the other taxa refer to the time span between the lowermost and uppermost occurrences. However, both kinds of ranges are treated identically by the software (see below). Due to the differences in the kind of age range, we refrain from analyses of ancestral-descendant relationships of individual taxa in particular trees (cf. Parins-Fukuchi, 2021).

Bayesian inference: The character-taxon matrix was also analyzed using Bayesian inference in MrBayes v3.2.2 (Ronquist et al., 2012). To do so, several multistate characters were recoded so as not to exceed a maximum of five character states per character in MrBayes. Character 55: states 4 and 5 were combined. Character 56: 0 for state 0, 1 for states 1–2, 2 for states 3–4, 3 for states 5–6. Character 64: 0 for states 0-2, 1 for states 3-5, 2 for states 6-8, 3 for states 9-B. Character 147: 0 for states 0–1, 1 for states 2–4, 2 for states 5–7, 3 for states 8–A, 4 for states B–C. Character 148: 0 for states 0–1, 1 for states 2–3, 2 for states 4–5, 3 for states 6–7. Character 217: as for character 147. Character 249: as for character 56. Character 88, states 4–5 were rescored as 3–4 (state 3 was not present in the original dataset).

The analysis (analysis 2) is based on the *Mk* character model of Lewis (2001). Additive characters were ordered using ctype. Default priors were used. The analyses were allowed to run with 4 chains (1 cold and 3 heated) for 20 Mgen (million generations) and sampled every 1000 gen. Convergence was ascertained using diagnostics obtained from "sump." Burn-in was set to 25%.

Tip-dating: We also conducted total-evidence dating using the fossilized birth-death (FBD) model (Stadler, 2010) as implemented in MrBayes v3.2.2 to estimate divergence times and determine whether any of the fossil taxa are directly ancestral to any other sampled lineage. Because the foregoing analyses had identified the taxa of interest as pan-xenosaurs, the analysis focused on that group. *Elgaria multicarinata* was used as the sole outgroup. In the first analysis (3a), fossil taxa were treated as terminal (i.e. no sampled ancestors were allowed), in order to compare the FBD model with the previous analyses. The analysis ran for 20 Mg. In the second analysis (3b), fossil taxa were allowed to be sampled ancestors. Because this analysis produced results at variance with all other analyses, it was allowed to run for 50 Mg, in order to be very certain about convergence. The dataset was the same as used above. We used the relaxed clock model IGR (Lepage et al., 2007). Similar results were achieved using the TK02 model (Thorne and Kishino, 2005), studied intensively by Simões et al. (2020), except that the relative positions of *Restes rugosus* and *Exostinus lancensis* were reversed; as this result conflicts with considerable character evidence amassed by Bhullar (2011) and reflected in the MP results, we tentatively prefer the IGR model. Additive characters were ordered as above.

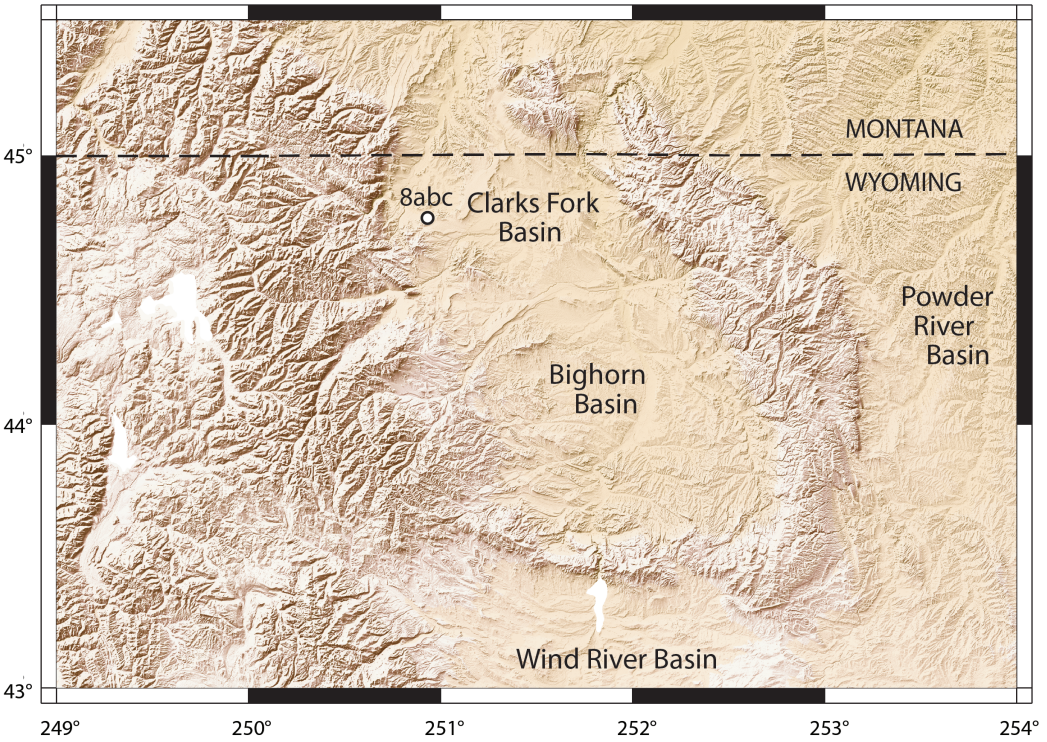

FIG. 1. Shaded relief map (based on Shuttle Radar Topography Mission 3 arcsecond/90 m digital elevation model) of the Bighorn Basin, Wyoming, showing the location of the 8abc limestone locality.

As there is no evidence for "diversified" sampling of extant taxa (Zhang et al., 2016), we set the sampling strategy prior to "random." The dataset covers six living species of *Xenosaurus*. Since Bhullar's (2011) work, several populations have been recognized as evolutionarily distinct or actually elevated to species status, and further species described (Lemos-Espinal et al., 2012; Woolrich-Piña and Smith, 2012; Nieto-Montes de Oca et al., 2017). The most recent genetic study suggests that as many as 18 species could be recognized (Nieto-Montes de Oca et al., 2017). Thus, we set the sampling probability prior to 0.33 (= 6/18).

The tree age prior (i.e., the age of the split between Pan-Xenosaurus and the outgroup, *Elgaria multicarinata*) was set to an offset exponential distribution with a mean of 75 Ma (mid-Campanian, earliest pan-xenosaur, from Longrich et al., 2012) and maximum of 100 Ma (oldest putative neoanguimorph, from Nydam, 2000).

Priors on species ages were set as uniform distributions on the lower and upper boundaries of the geochronologic range, as given above, except for the new taxon, which we took to have a fixed age of 55 Ma. Accordingly, we adopted the practice of coding the stratigraphic range of fossil species, where known from more than a single occurrence, as a uniform prior between first and last occurrence; this is not necessarily desirable, because it is equivalent to uncertainty in a single date, but alternative approaches have not yet been fully explored for the FBD model (Matzke and Wright, 2016).

Diversity analyses: Graphics and analyses make use of the phytools (Revell, 2012), paleotree (Bapst, 2012) and strap (Bell and Lloyd, 2015) packages for R v.4.0 (R Core Team, https://www.r-project.org). Raw species diversity curves for continuous data (precise ranges) were calculated using the function taxicDivCont. Species diversity curves are based on time-scaled trees, including cal3 and FBD trees, and calculated using the function phyloDiv or multiDiv. The continuous rather than time-binned versions of these functions were used because the temporal range of most species is fairly precisely known.

Unresolved polytomies in the consensus tree will bias toward higher diversity at older ages, because the participating lineages are extended back in time to the first-documented or first-diverging lineage (e.g., Brocklehurst et al., 2013). To circumvent this problem for FBD BI analyses, we made use of the large samples of trees from the posterior distributions saved in the tree (".t") files that are output by MrBayes. The values associated with each branch in the individual trees are in units of expected number of changes given the base rate of the clock, so by dividing these values (imported as edge lengths into the "phylo" objects in R) by the base clock rate (change/unit time) in the associated parameter file (".p") for the particular generation and run, branch lengths for these individual tree samples can be derived in units of time. Indeed, that is how MrBayes computes branch lengths in units of time for the consensus (F. Ronquist, personal commun., 2021). We were then able to plot diversity curves (lineage-through-time plots) for each of these trees individually using the function multiDiv.

Whether a particular species is ancestral to another in the phylogeny was assessed based on the unconstrained MP tree under the cal3 model, which distinguishes between budding (when the ancestor continues to live alongside the descendant) and anagenesis (when the ancestor becomes so transformed as to be recognized as a different species, the descendant). Under the FBD model with sampled ancestors (FBD-SA), the probability that a particular species is an ancestor was assessed by randomly sampling 1000 post-burnin trees from the posterior probability distribution and calculating the proportion of times that the branch length of each fossil species was 0; additionally, the output parameter files indicate the average proportion of ancestral species.

Material Examined

Comparative osteological specimens of Anguimorpha used in this study. Shinisauridae: *Shinisaurus crocodilurus* (MVZ 204291, SMF PH 84, 91, 93, 94); Xenosauridae: *Xenosaurus grandis* (MVZ 128947, 128948, 137627, 137786, 137798–137790, UMMZ 149608), *X. platyceps* (UF 45622, 54559); Anguidae: *Abronia deppei* (UTA R 5646), *A. mixteca* (UTA R-10277), *Anniella pulchra* (UF 51810), *Celestus costatus* (FLMNH 13254), *Diploglossus enneagrammus* (MVZ 191042), *D. monotropis* (MCZ 29682), *D. pleii* (CAS 200840), *Elgaria coerulea* (CAS 14509), *E. multicarinata* (YPM HERR 14098), *Gerrhonotus infernalis* (TMM-M7129, 7525), *Mesaspis moreletii* (YPM R13518), *Ophisaurus ventralis* (CAS 74296, 200896); Helodermatidae: *Heloderma horridum* (SDSNH 59469, YPM HERR 16804, 16820), *H. suspectum* (CAS 159494, SMF PH 135); Varanidae: *Lanthanotus borneensis* (SMF PH 336), *Varanus exanthematicus* (YPM HERR 10812).

Institutional Abbreviations

AMNH	American Museum of Natural History, New York
CAS	California Academy of Sciences, San Francisco
CM	Carnegie Museum of Natural History, Pittsburgh
MCZ	Museum of Comparative Zoology, Harvard University, Cambridge, Massachusetts
MVZ	Museum of Vertebrate Zoology, University of California, Berkeley, California
SDSNH	San Diego Natural History Museum, San Diego
SMF-PH	Paleoherpetology collection, Senckenberg Research Institute, Frankfurt am Main, Germany
UF	University of Florida Museum of Natural History, Gainesville
UMMZ	University of Michigan Museum of Zoology, Ann Arbor
USNM PAL	Paleontology collection, National Museum of Natural History, Smithsonian Institution, Washington, D.C.
UTA	University of Texas, Arlington, Texas
TMM	Texas Memorial Museum, University of Texas, Austin
YPM HERR	Herpetology collection, Peabody Museum of Natural History, Yale University, New Haven, Connecticut

RESULTS

Description and Comparisons of USNM PAL 768729

Maxilla: The left maxilla is nearly complete, lacking only its posterior end and part of the palatal flange at the anterior end (fig. 2). The facial process is broad, seven tooth spaces in length from its anterior margin to the lacrimal embayment. Its anterior margin curves rapidly dorsally, reaching an inflection point that marks the posterior extent of the external naris on the maxilla, whereupon it extends posterodorsally and medially (fig. 2A, B). The point, marking the extent of the nasal articulation on the maxilla, does not overhang the premaxillary process, as it does in most Anguidae (exceptions: *Anniella* and *Elgaria*), *Xenosaurus*, and *Shinisaurus*. The inflection point forms a laterally inflected corner, as in *Xenosaurus*. After reaching its apex, at midlength, the facial process maintains the same height but extends posterolaterally. A small embayment near its dorsal terminus marks the prefrontal articulation. The posterior end of the facial process is more or less vertical but shows a distinct posterior embayment for the lacrimal. The lacrimal articulation is bounded both by this embayment and by a more posterior inflection point in the lateral maxillary wall. The posterior inflection point is absent in extant *Xenosaurus* and many anguids (*Celestus* spp., *Mesaspis* spp., *Ophisaurus attenuatus*), but is found in other anguids (*Elgaria coerulea, Ophisaurus ventralis*), *Restes rugosus*, *Heloderma*, *Eurheloderma gallicum*, *Lanthanotus borneensis*, and *Estesia mongoliensis* (Norell et al., 1992: fig. 6; K.T.S., personal obs.). Between these boundaries, the dorsal edge of the facial process has an elongate, shallow facet that is slightly broader and deeper posteriorly. Posterior to the lacrimal

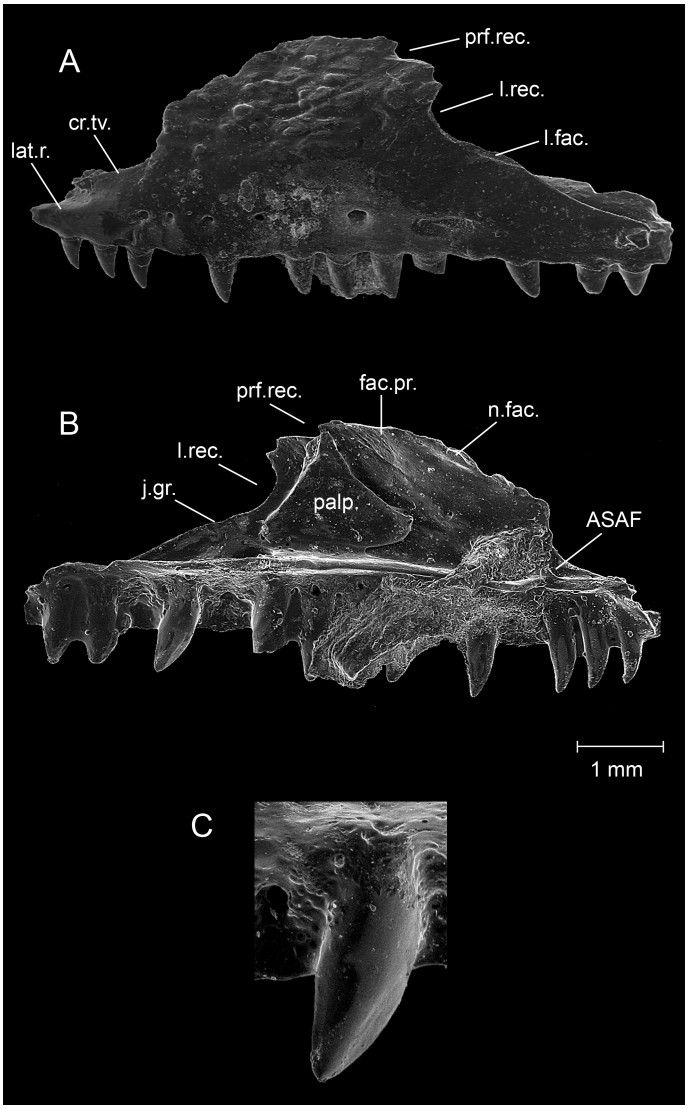

FIG. 2. Nearly complete left maxilla of USNM PAL 768729. **A,** lateral and **B,** medial views. Medial view also shows the palpebral, which remained attached to the maxilla. **C,** Close-up of third (preserved) maxillary tooth from rear. Abbreviations: **ASAF,** anterior superior alveolar foramen; **cr.tv.,** crista transversalis; **fac.pr.,** facial process; **j.gr.,** jugal groove; **l.fac.**, lacrimal facet; **lat.r.,** lateral ridge (= crista lateralis); **l.rec.,** lacrimal recess; **n.fac.,** nasal facet; **palp.**, palpebral; **prf.rec.,** prefrontal recess.

facet the lateral wall of the maxilla is sharp edged and decays smoothly in height; it is shallowly concave in lateral view and decays so strongly that the jugal groove is partly exposed in lateral view. A row of seven labial foramina (the fifth filled with sediment) is located above the jaw parapet. Dorsal to these foramina the lateral surface of the facial process is moderately but irregularly rugose; epidermal scale boundaries could not be ascertained. A few tiny foramina are scattered among the rugae. The whole facial process is medially folded about a low, oblique

axis that is in line anteriorly with the lateral ridge on the premaxillary process and terminates at the posterior projection that marks the boundary between the lacrimal and prefrontal embayments, i.e., at a point continuous with a presumed canthal crest of the prefrontal. Ventral to this axis the facial process is directed laterally; dorsally the process is directed anteriorly, dorsally, and laterally. The folding does not create a distinct ridge. The medial surface of the facial process is mostly smooth. A strong nasolacrimal ridge (Smith and Gauthier, 2013) is essentially absent, except perhaps ventrally near the palatal shelf (where the bone is covered by adhering sediment that is not easily removed).

The palatal shelf of the maxilla is dorsoventrally thin (fig. 2B) and mediolaterally wide, projecting medially a considerable distance beyond the bases of the teeth. In this respect it is similar to the palatal shelf of *Xenosaurus* as well as gerrhonotine, diploglossine, and annielline anguids; it is narrow in *Shinisaurus* and many *Varanus* spp., and wide only anterior to the palatine articulation in *Lanthanotus borneensis* and *Heloderma* spp. Anterior to the superior alveolar foramen (SAF), into which plunge the superior alveolar branch of V2 and the maxillary artery (Oelrich, 1956), the dorsal surface of the shelf is flat and slopes slightly laterally (unlike in *Shinisaurus*, where it slopes medially). Anteriorly, the palatal shelf begins to curve medially, following the trend of the lateral margin of the maxilla, but the shelf is broken medially beyond the level of the anterior margin of the facial process. The crista transversalis, extends anteriorly and slightly medially from the anterior base of the facial process, separating the premaxillary portion of the palatal shelf from the posterior portion. The anterior superior alveolar foramen (ASAF), through which passes the superior alveolar nerve and maxillary artery, opens just anterior to the base of facial process and medial to the crista, as in extant *Xenosaurus*, *Shinisaurus* (Smith, 2009; Bhullar, 2011) and certain extinct platynotans like *Parasaniwa* (Gao and Fox, 1996: fig. 33B) and *Palaeosaniwa* (Gao and Fox, 1996: fig. 38D). The palatine process of the maxilla, the SAF, and the posterior end of the facial process occur at approximately the same anteroposterior level. The anterior end of the palatine process curves sharply away from the trend of the medial margin of the palatal shelf, achieving maximal width in about one tooth space. Its anterior margin is thus more abrupt than in most *Xenosaurus grandis* (MVZ 137788 comes close), *X. platyceps*, most anguids (*Ophisaurus ventralis* and *Elgaria coerulea* were exceptions), Varanidae, and Helodermatidae. The medial edge of the process is straight and slightly oblique to the trend of the palatal shelf. The process gradually decays in width posteriorly, slightly more rapidly beyond the end of the palatine articulation. The articulation itself is a lenticular, dorsoventrally thin facet, approximately two tooth spaces in length, which faces medially and slightly dorsally and is bounded dorsally and ventrally by small ridges of bone. We infer that the neurovascular structures that enter the SAF divided or separated shortly upon entering the maxilla. One division turned immediately to exit laterally through the ultimate labial foramen, which is visible when viewing the SAF in dorsomedial aspect. Another division passed deep into the maxilla and ran anteriorly; this division was separated from a more dorsal division, which runs immediately below the palatal shelf, by a small sheet of bone. This sheet is just barely visible in dorsal view. The SAF opens posteriorly because the dorsal surface of the maxilla is depressed behind it. This depression forms a trough that is continuous posteriorly

with the deepening jugal groove, which widens slightly posteriorly. The SAF and jugal groove are not continuous in most anguids (including gerrhonotines, anguines, diploglossines, and primitive glyptosaurines like *Odaxosaurus piger*), nor in *Xenosaurus* spp. or *Shinisaurus*.

The premaxillary process is not well preserved. It possesses a crista lateralis (Bhullar, 2010). The crista transversalis (Smith, 2006) is considerably taller, at least posteriorly, where it is visible in lateral view. The premaxillary process was weakly excavated between these two ridges. It is broken medial to the crista transversalis.

Dentition: Fifteen maxillary teeth are preserved (fig. 2B), and approximately two more might have been present at the posterior end of the tooth row. There is no evidence of corrosion to the tooth surfaces (cf. Smith et al., 2021). All teeth are simple and unicuspid, unlike those of *Xenosaurus* (Gauthier, 1982), but they vary slightly in morphology from anterior to posterior. The first tooth is slender, but tooth girth increases rapidly posteriorly; the fourth tooth was probably at near-maximum size for the toothrow, to judge by its alveolus. The shafts of anterior teeth are straight, but their tips are somewhat recurved (especially the first two); posterior to the eighth, the teeth are only slightly recurved. The bases of middle and anterior teeth are essentially parallel sided, and apical tapering is wholly confined to the crown; the last four teeth expand slightly from base to the level of the jaw parapet, whereafter the crowns taper. This flaring of the teeth at midshaft is a similarity shared with *Entomophontes* spp. (Smith and Gauthier, 2013), especially *E. hutchisoni*, but not with other extant anguimorphs; some taxa like the anguid *Ophisaurus acuminatus*, may have strong mesial and distal cutting edges, but they do not flare (Klembara and Čerňanský, 2020). All teeth show some development of mesial and distal carinae, although those on the anterior teeth are slight, scarcely more than longitudinal angulations on the mesial and distal aspects of the teeth. Even by the ninth tooth they are poorly developed. The most extensive, preserved carinae are on the 12th tooth (fig. 2C); even so, tooth cross-sectional shape is weak. The teeth are fairly high crowned, with about 50% of their height protruding below the parapet of the jaw, except at the posterior end of the jaw, where the teeth, in addition to being absolutely shorter, are relatively shorter crowned. The middle teeth of the tooth row have a height of about 1.14 mm (measured vertically from the base of the nutritive foramen to the apex of the crown).

Jugal: The left jugal is well preserved but lacks the ends of its anterior and temporal rami (fig. 3). The exposed lateral surface is sculptured, but unlike on the maxilla, the boundaries of polygonal epidermal scales can be discerned, at least along the orbital margin, as linear depressions that surround raised patches (fig. 3A). Among anguimorphs, a sculptured jugal is also found in *Xenosaurus, Shinisaurus*, and *Heloderma*, and Gao and Fox (1996) stress the widening and sculpture of the ascending ramus. The sculptured patches have undulose surfaces and are pierced in places by foramina. A ventral row of five larger foramina occurs along the ventral margin of the suborbital row of scales; a set of five generally smaller, less obviously colinear foramina opened deep to the suborbital scale row. An elongate impression marks where the jugal was in articulation with the posterior process of the maxilla. The articulation surface is strongly demarcated posteriorly, less well so anteriorly. The dorsoventral extent of the overlap decreases posteriorly and has a distinct kink at midlength. The

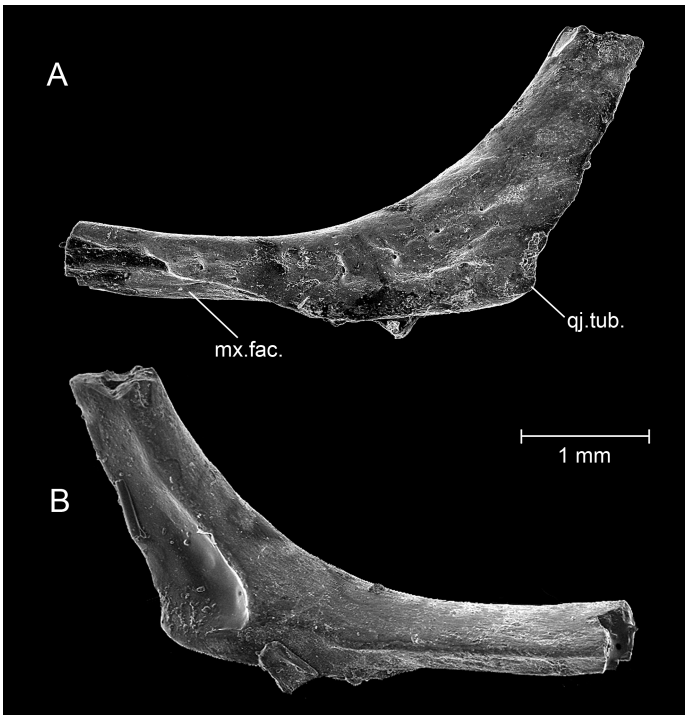

FIG. 3. Right jugal of USNM PAL 768729. **A,** lateral and **B,** medial views. Abbreviations: **mx.fac.,** maxillary facet; **qj.tub.,** quadratojugal tubercle.

overlap surface ceases to be visible in lateral view about 2 mm anterior to the quadratojugal tubercle. That tubercle is blunt, similar in size to that of *Ex. lancensis* (Gao and Fox, 1996: fig. 27E); it is (poorly) defined dorsally by a slight concavity of the posterior margin of the bone. The ascending or temporal ramus of the jugal rises at an angle of ~58° with respect to the suborbital ramus, curving also slightly medially. Its lateral surface is much smoother than that of the suborbital ramus.

In medial view the jugal presents a continuous ridge roughly parallel to the orbital margin (fig. 3B). The ventral surface of this ridge on the suborbital ramus is an articulation surface inserting in the jugal groove of the maxilla; the ridge is located below the dorsoventral midpoint of this ramus. This surface continues posteriorly for nearly 1 mm beyond the point where it ceases to be visible in lateral view. Near the posterior end of this surface there is a kink in the medial ridge, which indicates the location of the ectopterygoid articulation. The medial ridge then shows another inflection point, marked by a small, medial tubercle. The posteromedial face of the ascending ramus—posterior to the medial ridge—is deeply excavated, especially ventrally. For most of the preserved extent of the ramus, the ridge is located at the anteroposterior midpoint (not fully compatible with the types of Čerňanský et al., 2014). A small foramen penetrates the jugal in this fossa, well above the ventral margin of the bone.

The orbital face of the jugal is transversely flat anteriorly but becomes slightly convex near the angle of the jugal and finally broadly rounded toward the end of the ascending ramus (fig. 3B). It

is relatively narrow for most of its length, achieving maximum mediolateral width at the junction of the two rami. No foramen pierces the orbital face of the jugal on its preserved portion.

Palpebral: The left palpebral is inextricably stuck to the medial surface of the facial process of the left maxilla and is seen primarily in dorsal view (fig. 2B). The lateral edge faces ventrally, as it is preserved, and the anteromedial edge faces more or less posteriorly. In dorsal aspect it has the form of an equilateral triangle; thus, the posteromedial and posterolateral processes are subequal in length, although the latter is distinctly blunter and more robust. The equilateral shape and short, bluntly terminating posterolateral corner of the palpebral are features shared uniquely with *Xenosaurus*. Most of the element is dorsoventrally thin. However, much of the anteromedial edge is thickened, and viewed end-on there is a shallow longitudinal sulcus or facet. The posteromedial corner, however, like the entire posterior edge, is dorsoventrally thin and sharp. The medial margin is straight and does not show the S-shape typical of extant *Xenosaurus* (Bhullar, 2011). Like in *Xenosaurus*, *Shinisaurus*, and *Varanus*, but unlike in Anguidae, the posterior margin is concave.

Coronoid: The coronoid, on which various portions of the jaw adductor musculature insert (Haas, 1960), is preserved in articulation with the other post-dentary bones (fig. 4). It is medially concave in dorsal view and straddles the surangular. The tip of the coronoid is a mediolaterally compressed and posteriorly inflected, a feature encountered in North American *Ophisaurus* (*O. attenuatus*, some *O. ventralis*) and *Shinisaurus*. The tip is completely flat medially, but it bears a ridge laterally that extends ventrally and somewhat anteriorly to form the anterior margin of a fossa. The posterior edge of the tip of the coronoid extends nearly ventrally at first, then posteroventrally at an angle of ~44° to the vertical, forming a strong ridge on the posteromedial process. A tiny flange extends anteriorly along the prearticular from the ventral end of the posteromedial process. More conspicuous, however, is the strong posterior flange that extends posteriorly over the prearticular and surangular along the entire length of the posteromedial process. This flange is pierced by a tiny foramen at about midheight. The posterior margin of the flange is undulating. This flange also wraps dorsally over the apex of the surangular to form the floor of the fossa; its ventral margin is notched for the anterior surangular foramen (see below).

In medial view the coronoid is deeply concave ventrally between the posteromedial process and the much longer anteromedial process, whose tip is broken. The medial surface of the latter shows a conspicuous facet at midheight whose dorsal margin is roughly horizontal and that marks the medial overlap of the splenial. Ventrally, then, the anteromedial process of the coronoid inserted between the splenial (medially) and the anterior processes of the surangular and prearticular (laterally). On its lateral surface above the level of the facet the anteromedial process articulated on the subdental shelf of the dentary. The coronoid process of the dentary then extends posterodorsally beyond this and inserts in the crotch between the anterolateral and anteromedial processes of the coronoid. The tip of the anterolateral process is broken, but if its dorsal and ventral margins maintained their trends, very little of the process is missing.

Splenial: The splenial, like the dentary, is not preserved, and it seems likely that these elements were dissociated from the postdentary elements prior to burial. However, facets on

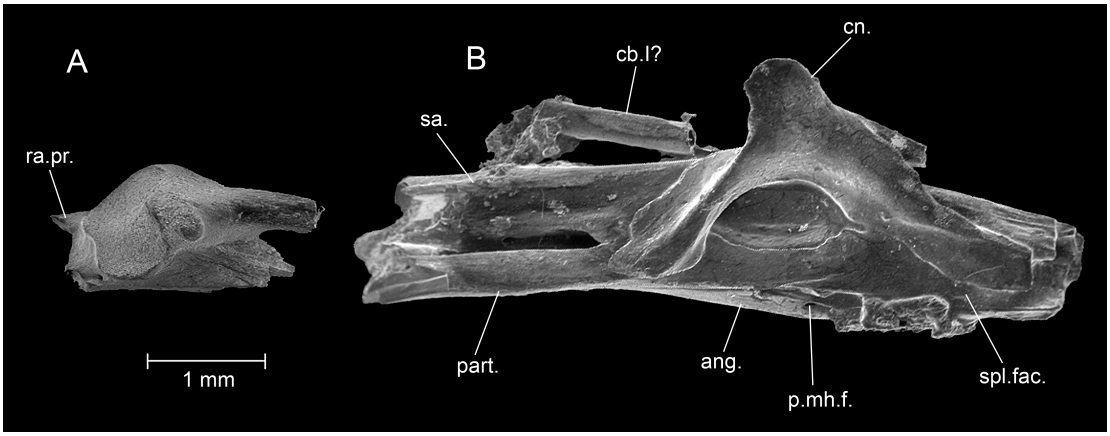

FIG. 4. Partial left mandible of USNM PAL 768729 in medial view. **A,** Articular region, with broken retroarticular process. **B,** Middle region, including coronoid and angular. Abbreviations: **ang.,** angular; **cb.I,** ceratobranchial I; **cn.,** coronoid; **part.,** prearticular; **p.mh.f.,** posterior mylohyoid foramen; **ra.pr.,** retroarticular process; **spl.fac.,** splenial facet.

the remaining bones (fig. 4) permit the reconstruction of the splenial's posterior end. It overlapped the anteromedial process of the coronoid and probably ended shortly before reaching the point where the prearticular dives under the process. From there, its posterior margin extended first ventrally, then arced posteroventrally, inserting between the prearticular and angular. Its posterior-most extent was level with the apex of the coronoid. Its ventral extent is marked by a deep, horizontal sulcus between angular and prearticular, which shallows anteriorly.

Angular: This bone forms the ventral margin of the jaw beneath the coronoid (fig. 4). It extends anteriorly to the end of the mandible as it is preserved and would have terminated well anterior of the end of the toothrow. It is pierced by the posterior mylohyoid foramen at a transverse level just anterior to the apex of the coronoid, and it is around this point that the angular achieves maximal medial exposure. Posteriorly, it rotates laterally and is applied almost exclusively to the ventral margin of the mandible. Like the ventral margin itself, the angular is shallowly ventrally concave behind the coronoid process. It has a tabular form, with nearly parallel medial and lateral margins. These margins converge posteriorly, however, and the bone terminates in a sharp point approximately level with the anteroposterior midpoint of the adductor fossa.

Prearticular: The long anterior process of this element runs lateral to the anteromedial and posteromedial processes of the coronoid and is overlapped ventrally by the angular (fig. 4). The prearticular extends as far as the preserved anterior end of the mandible, significantly in front of the posterior margin of the dentary (however defined). It is sutured with the surangular both medially and laterally. The medial suture is interrupted by the adductor fossa, but the anterior portion of the medial convergence of the two bones is visible behind the posteromedial process of the coronoid, unlike in most anguimorphs, except *Xenosaurus* spp., some gerrhonotines, and the diploglossine *Celestus costatus*. This suture is also visible between the

anteromedial and posteromedial processes of the coronoid; there, it is dorsally concave. Posterior to the tip of the ventromedial process of the coronoid, the prearticular forms a strong, relatively sharp medial shelf. This shelf extends posteriorly for the full length of the adductor fossa and contributes to the strong ventral flatness of the posterior portion of the mandible.

The adductor fossa is dorsoventrally deep but mediolaterally narrow (restricted; fig. 4), as in many anguimorphs (except *Shinisaurus*). A canal within the prearticular opens into the posterior end of the fossa. This canal is visible at the broken posterior end of the main mandibular section and was once filled by Meckel's cartilage, which also occupied the floor of the adductor fossa. Some porous and friable material of the same color as the bone is found within the canal at its broken posterior end; this material could represent the calcified cartilage.

The prearticular, like the surangular, is fully united posteriorly with the endochondral articular bone (fig. 4). The articular strongly overhangs the medial margin of the prearticular beneath the articular fossa. The prearticular also formed the retroarticular process, which is broken near its base. The foramen chorda tympani, which conveys part of the facial nerve into the mandible, pierces the retroarticular process near its medial edge just behind the articular fossa. The preserved portion of the retroarticular process was flat ventrally but was dorsally concave, with medial and lateral bounding ridges.

Surangular: Anteriorly, the surangular was overlapped dorsally by the coronoid and the coronoid process of the dentary, and laterally by the surangular process of the dentary. The latter, triangular process extended slightly more posteriorly than the former process and was dorsoventrally short. Clear articulation facets on the surangular indicate that the angular notch of the dentary (the space between the surangular and angular processes) was deeper than the surangular notch (the space between the coronoid and surangular processes) and that the angular process of the dentary was the least posteriorly extensive of the three processes that constitute the posterior margin of the dentary. Just beneath the coronoid on the lateral side, and level with its apex, is the anterior surangular foramen. Beneath the ventral concavity of the coronoid on the medial side is a deep concavity in the surangular, a feature shared uniquely with *Xenosaurus* among extant anguimorphs. The surangular forms the lateral margin of the adductor fossa (fig. 4). Lateral to the superior margin of the bone is a flat, elongate, laterally sloping surface that extends from the suture anteriorly with the coronoid to the edge of the articular fossa. This surface is bounded ventrally by a moderately sharp ridge, below which the surangular is weakly convex and extends ventromedially. The surangular projects medially over the adductor fossa near its anterior end, partially obscuring it in dorsal view and contributing to its "restriction." Just above this projection is a longitudinal impression that extends for much of the length of the adductor fossa but is best developed near its midpoint; this impression appears to be unique among anguimorphs. The transversely rounded dorsal margin of the surangular becomes wider and dorsally flatter posteriorly. The posteromedial end of the surangular is marked by a strong tubercle.

Articular: This endochondral element is bilobate in dorsal view (fig. 4). The lateral portion is moderately concave in all directions and separated from the medial portion by a mediolaterally broad, longitudinal ridge. The lateral portion is much larger than the medial portion

and also deeper and more deeply concave; these facts suggest that the quadrate had a larger and more bulbous lateral lobe than medial lobe. The posterior boundary between the articular and prearticular is more clearly marked posteriorly than the anterior boundary between articular and surangular. However, the surangular projects posteriorly at the point where it meets the ridge divided the lateral and medial portions of the articular. Along the posterior margin of the articular is a small posterior projection that is located lateral to said ridge.

Ceratobranchial I: A short (1.5 mm) section of a slender, hollow, rod-shaped element is preserved in association with the surangular (fig. 4). It probably represents ceratobranchial I (the only ossified element of the squamate hyoid apparatus: Cope, 1892), which unlike the epipterygoid is hollow.

Dorsal vertebra: Based on its proportions and the shape of the synapophysis, the sole preserved vertebra is probably an anterior dorsal vertebra (fig. 5). It measures 2.4 mm in length along the base of the centrum. The bone is generally well preserved, but portions of the postzygapophyses, the right prezygapophysis, and the neural spine are broken (fig. 5A). The dorsal surface of the left prezygapophysis is inclined medially. From its medial anteromedial end at the junction with the neural arch, the margin turns fairly sharply posterolaterally, then curves smoothly posteromedially back toward the neural arch (the slight irregularities in curvature are due to erosion of the edge of the prezygapophysis). Thus, the anterior-most portion of the prezygapophysis lies close to its junction with the neural arch. The transition from the dorsal surface of the prezygapophysis to the neural arch is smooth; however, a distinct surface for articulation of the postzygapophysis on the neural arch (a zygosphene) is not in evidence. On each side of the nearly vertical, inner surface of the neural arch medial to the postzygapophyses, however, is a distinct, dorsoventrally short articular surface that would have contacted the anterior portion of the neural arch medial to the prezygapophysis. That is, the kind of weak, accessory vertebral articulation found in many Squamata (Gauthier et al., 2012, character 468(1)) is found also in this species. The lateral margins of the postzygapophyses are poorly preserved.

The neural arch is subtly inflated between the prezygapophyses, and the neural canal concomitantly slightly expanded. Its anterior-most portion on the midline is broken, but enough remains to show that the neural spine was absent anteriorly but begins to rises abruptly near the level of the posterior end of the prezygapophysis (fig. 5A). The spine arises abruptly. Unfortunately, its dorsal portion is damaged anteriorly. Posteriorly, its dorsal edge is nearly horizontal (fig. 5B). The spine is low by comparison with most extant anguimorphs in the middle and posterior dorsal vertebrae, except the semifossorial taxon *Anniella* and crevice-dwelling *Xenosaurus* and other cryptic forms like certain anguines (Čerňanský et al., 2019) and *Elgaria multicarinata* (San Bernardino County Museum specimen number A500-2327). Posteriorly, the neural spine increases in mediolateral thickness. At its posterodorsal tip, a small divot is excavated that appears natural; similar divots in modern anguimorph vertebrae are filled with small bodies of calcified cartilage. The posterior tip of the spine does not extend beyond the posterior margin of the postzygapophyses, and each half of the posterior margin of the neural arch is only weakly concave, unlike in most anguimorphs.

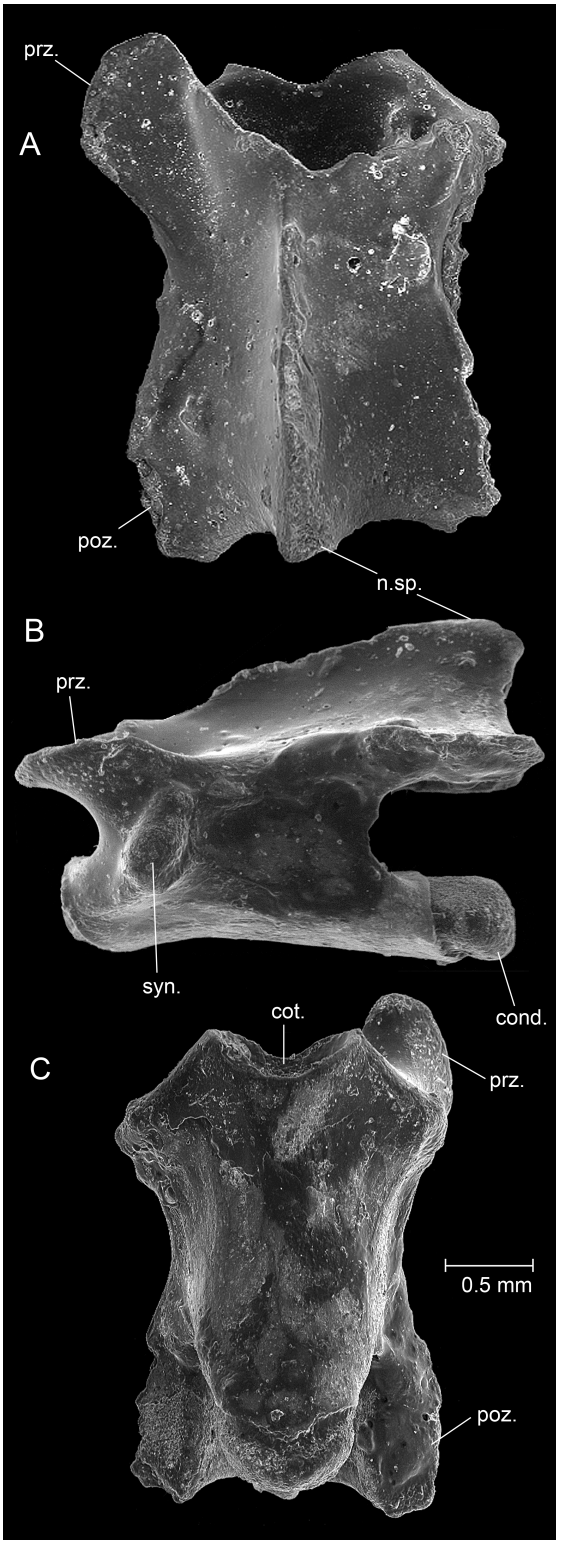

The neural canal is large, dorsoventrally taller than the centrum, which is somewhat compressed. In lateral aspect the boundary of the cotyle anteriorly and of the centrum exclusive of the condyle posteriorly are slightly anteriorly inclined but primarily vertical. Ventromedially, however, they tend to curve posteriorly (fig. 5B). Thus, the cotyle in ventral view is anteriorly concave. The dorsal edge of the cotyle is also anteriorly concave. The centrum is depressed in comparison with adult *Shinisaurus crocodilurus* and *Xenosaurus grandis*. The ventral surface of the centrum is concavoconvex (fig. 5C). It is straight for most of its length in midsagittal section, but a ventral deflection of the ventral portion of the cotyle gives it a concave outline overall. In transverse section, it is concave, slightly more acutely so just posterior to the synapophysis. A tiny subcentral foramen is set in a subtle longitudinal depression on the right side of the centrum, approximately one-fourth of the way posteriorly.

The synapophysis is elliptical, with a slightly more bulbous ventral portion, and is primarily located at a coronal level dorsal to the centrum (fig. 5A). Although damage to the left prezygapophysis makes it difficult to ascertain, it is likely that the synapophysis was only scarcely visible in dorsal view or was obscured entirely by the prezygapophysis.

Scapulocoracoid: Only a small portion of this element is preserved. The scapula and coracoid are indistinguishably fused (fig. 6), suggesting this individual was sexually

FIG. 5. Dorsal vertebra of USNM PAL 768729. **A,** dorsal, **B,** left lateral, and **C,** ventral views. Note the low neural spine. Abbreviations: **cond.,** condyle; **cot.,** cotyle; **n.sp.,** neural spine; **poz.,** postzygapophysis; **prz.,** prezygapophysis**; syn.,** synapophysis.

mature (Maisano, 2002). The glenoid fossa is saddle shaped. The scapular portion is pierced by the scapular foramen along its thickened posterior margin just dorsal to the glenoid fossa. Anterodorsal to the fossa, just above the probable former location of the scapulocoracoid suture, the lateral surface of the scapula shows a broad swelling capped by a tubercle. The posterior margin of the scapulocoracoid fenestra is preserved well above the level of the glenoid fossa. Directly anterior to the middle of the fossa is preserved the thickened posterior margin of the coracoid foramen. An anterior (or primary) coracoid fenestra is not preserved.

Ontogenetic stage and size: The small size of USNM PAL 768729 is remarkable. As noted above, its maxilla measures only 3.3 mm from the anterior base of the facial process to the notch on its posterior margin, and teeth in the middle of the jaw are 1.14 mm tall. Accordingly, the animal represented by USNM PAL 768729 had a SVL of 54.4 mm with 95% C.I. 50.9–58.2 mm (error on the slope; fig. 7). In her careful study of terminal fusions of skeletal elements in lizards, Maisano (2002) did not specifically look at fusion of the postdentary elements, but indistinguishable fusion of the scapula and coracoid suggests the animal was sexually mature (Maisano, 2002). In contrast, the proposed stem-xenosaur *Entomophontes incrustatus* commonly has teeth >2.2 mm, which implies an SVL >100 mm (using the same model). Extant species of *Xenosaurus* typically have maximum SVL between 100 and 130 mm (Lemos-Espinal et al., 2012). Thus, the species represented by USNM PAL 768729 was about half the size of extant species of *Xenosaurus*.

Phylogenetic Relationships

Under MP, three equally most-parsimonious trees were recovered in both the unconstrained analysis (1a) and the analysis with a molecular backbone (1b). In each, USNM PAL 768729 forms a clade together with *Entomophontes incrustatus* and *En. hutchisoni* (fig. 8A). Bootstrap support for this clade is 65% in analysis 1a and 70% in analysis 1b. This is a rather remarkable inference considering that USNM PAL 768729 and *Entomophontes* share only a single element in common: the maxilla. This clade is the basalmost clade of Pan-Xenosaurus, and bootstrap support for a Pan-Xenosaurus so constituted is <50% in analysis 1a and 76% in analysis 1b. Apart from the addition of this basalmost clade, the topology of Pan-Xenosaurus otherwise corresponds to the results of (Bhullar, 2011), with *Restes rugosus*, *Exostinus lancensis*, and *Ex. serratus* successively crownward taxa on the stem of *Xenosaurus*, supporting the contention that *Exostinus* is paraphyletic as presently constituted (Bhullar, 2011). Crown *Xenosaurus* is strongly supported in both analyses (bootstrap 99% in each). Branch length was substantially lower in the unconstrained analysis: 903 vs. 929 steps.

Thirteen unambiguous synapomorphies (under ACCTRAN and DELTRAN) support the monophyly of Pan-Xenosaurus as recognized here: dentigerous arc of premaxilla tall (3: 0 → 1), more vertical lateral edges of rostral body of premaxilla (4: 0 → 1), premaxillary ethmoid canals bony (6: 0 → 1), >2 colinear anterior foramina in main row on premaxilla (7: 0 → 2), at least 3 anterior foramina dorsal to main row on premaxilla (8: 0 → 3), maxillary labial foramina subequal in size (53: 0 → 1), posterior portion of nasal facet of maxilla folded towards the verti-

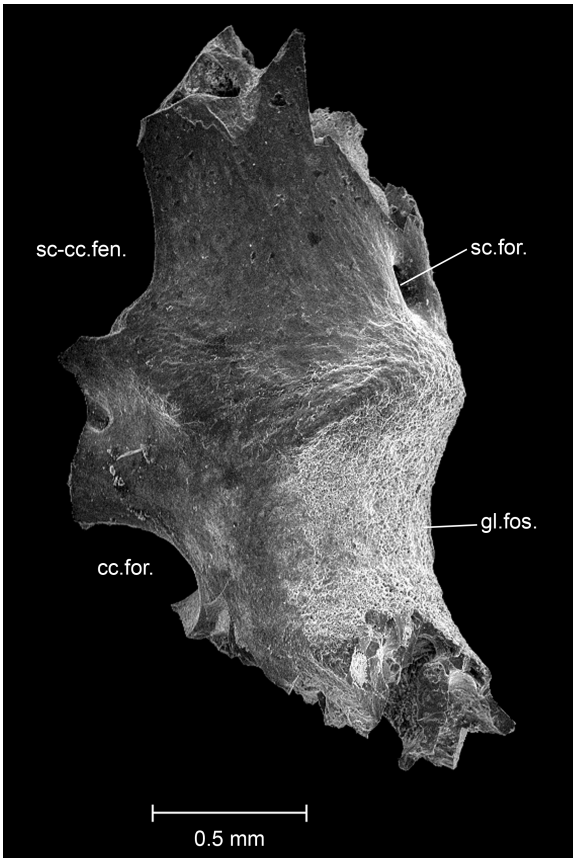

FIG. 6. Central fragment of left scapulocoracoid of USNM PAL 768729. The scapula and coracoid are indistinguishably fused. Abbreviations: **cc.for.,** coracoid foramen; **gl.fos.,** glenoid fossa; **sc-cc.fen.**, scapulocoracoid fenestra; **sc.for.,** scapular foramen.

cal (59: 0 → 1), shape of palpebral a short triangle (109: 0 → 1), foramen in jugal adductor surface (130: 0 → 1), parietal foramen close to frontoparietal suture (152: 0 → 1), Meckel's groove restricted by supramecklelian lip (191: 0 → 1), posterior decline in dentary tooth height reduced (196: 0 → 1), and low neural spines at least in one-third of vertebral column (214: 0 → 1). Three more are present only under DELTRAN, and 56 more only under ACCTRAN. The highly arcuate rostral margin of the premaxilla recognized by Smith and Gauthier (2013) as a potential synapomorphy of *Entomophontes* and *Xenosaurus* is not found on this list, because the plesiomorphic condition is present in *Exostinus serratus* (Bhullar, 2010) and the premaxilla is unknown in *Ex. lancensis* and *Restes rugosus* (Bhullar, 2011).

Four unambiguous synapomophies support the monophyly of *Entomophontes* spp. and USNM PAL 768729: relative length of facial process of maxilla rises (55: 3 → 5), relative height of facial process decreases (56: 4 → 6), shafts of dentary teeth increase in diameter posteriorly (197: 0 → 1) (unknown in USNM PAL 768729), strong mesial and distal carinae on cheek teeth (275: 0 → 1). Four more are present only under ACCTRAN.

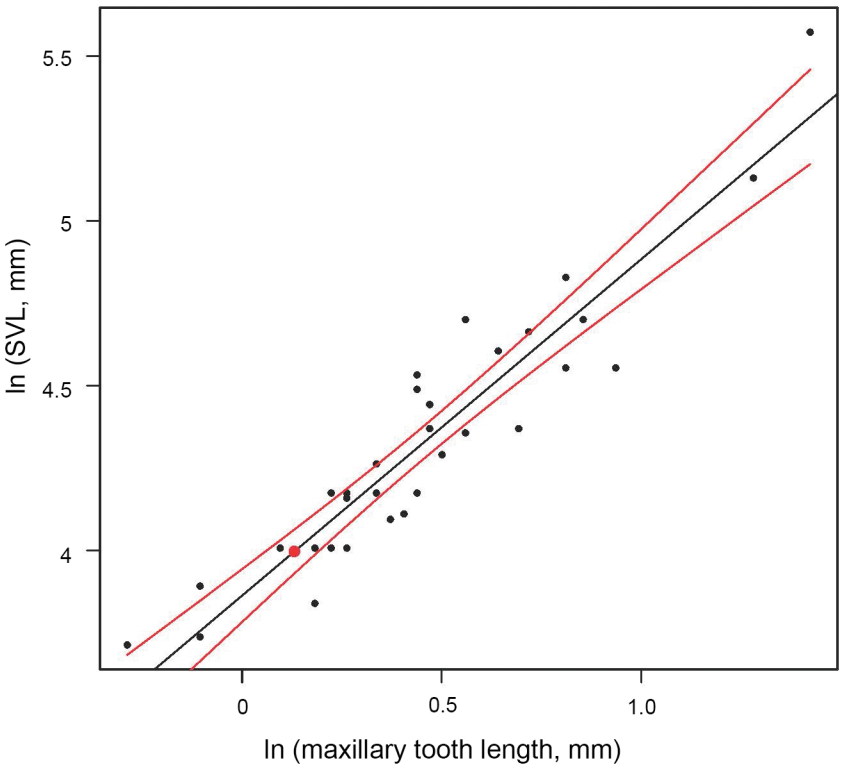

FIG. 7. Relation between maxillary tooth length and snout-vent length (SVL) in iguanid lizards (log-log space). Ordinary least squares regression was used to predict SVL from tooth length. Iguanid lizards were preferred to anguimorphs because the broad spectrum of body size covered by available skeletons did not require extrapolation. Red dot represents prediction for USNM PAL 768729.

Three unambiguous autapomorphies of USNM PAL 768729 are: steeper rise of lacrimal recess of maxilla (46: 0 → 1), posteriormost labial foramina of maxilla larger (53: 1 → 0), maxillary osteoderms as low mounds (62: 1 → 2). Five more are present only under DELTRAN.

Ten unambiguous synapomorphies support the monophyly of more crownward Pan-Xenosaurus, including *Exostinus* spp. and *Restes rugosus*: bicuspid teeth (1: 0 → 2) (more on this character in the discussion), anterior end of lacrimal recess of maxilla more posterior (45: 1 → 0), maxilla supradental thickening strong (52: 1 → 2), maxillary osteoderms as low mounds (62: 1 → 2), frontals fused (91: 0 → 1), frontal osteoderms variously platelike and domed (97: 0 → 2), palpebral with fused osteoderms (111: 0 → 1), palpebral medial margin with S-curve (113: 0 → 1), lacrimal large (114: 0 → 1), groove anterior to coronoid facet of dentary deep and long (186: 0 → 1). An additional 11 synapomorphies support this clade under ACCTRAN and an additional nine under DELTRAN.

Cal3 found strong evidence for only a single species being ancestral to others (table 1). *Exostinus lancensis* was interpreted in 90% of the trees in the sample as a direct ancestor (via budding) of more crownward pan-xenosaurs. Two other species, *Entomophontes incrustatus* and *Ex. serratus*, were interpreted as ancestors (via budding) in one-fourth to one-fifth of

TABLE 1. Frequencies with which particular fossil species are interpreted as ancestors (via budding or anagenesis) in the cal3 and FBD with sampled ancestors (FBD-SA) models. The cal3 model was applied to trees consistent with the molecular constraint. The FBD-SA model is based on trees sampled from the posterior probability distribution.

Species	cal3 (budding or anagenesis)	FBD-SA
Blutwurstia oliviae	0.01	0.28
Entomophontes incrustatus	0.19	0
Entomophontes hutchisoni	0	0.252
Exostinus lancensis	0.9	0.346
Restes rugosus	0	0.33
Exostinus serratus	0.25	0.286
	1.35	1.494

the trees. BI (analysis 2) yielded a tree in which the topology of Pan-Xenosaurus was nearly the same as in MP (fig. 8B). Only within (crown) *Xenosaurus* was there a loss of resolution. Support for a clade composed of *Entomophontes* and USNM PAL 768729 was relatively low (58% posterior probability), as it was for Pan-Xenosaurus (51%). Support for *Exostinus serratus* + *Xenosaurus* is high, in fact higher than for the monophyly of *Xenosaurus*. The posterior probability of the clade Pan-Xenosaurus to the exclusion of *Entomophontes* and USNM PAL 768729 was 0.93.

In Bayesian analyses using the fossilized birth-death process, USNM PAL 768729 is inferred to be a member of a monophyletic Pan-Xenosaurus. Nevertheless, the results are illuminating. In the analysis excluding possible ancestors (3a), similar relationships are obtained as for analyses 1 and 2, except that it is unresolved whether *Restes rugosus* or *Exostinus lancensis* is more closely related to crownward Pan-Xenosaurus (fig. 8C). If taxa are allowed to be ancestors (analysis 3b), then a result obtains that is at variance with the results of all other analyses. Namely, *Ex. lancensis* is inferred to be the basalmost known member of Pan-Xenosaurus, while *R. rugosus, Entomophontes* spp., USNM PAL 768729, and more crownward Pan-Xenosaurus form an unresolved polytomy. Support for this clade of Pan-Xenosaurus exclusive of *Ex. lancensis*, however, is poor (posterior probability 0.57), and only small changes in the assumptions (assuming *R. rugosus* has a point occurrence at 57 Ma instead of a range occurrence from 59–57 Ma) are needed to revert the topology to one in which *Entomophontes* and USNM PAL 768729 form the basalmost clade of Pan-Xenosaurus.

A sister-group relationship between the species represented by USNM PAL 768729 and *Entomophontes* thus has relatively strong support under MP and that clade is generally inferred under MP and BI as the basalmost known member of Pan-Xenosaurus. Two species, *En. incrustatus* and *En. hutchisoni*, have already been described for *Entomophontes* (Smith and Gauthier 2013). Both species differ strikingly from USNM PAL 768729 in the extent of osteoderm development on the maxilla—in other words, in external appearance. On the basis of the strikingly different appearance we feel justified in naming a new genus as well as species for USNM PAL 768729.

SYSTEMATICS

Squamata Oppel, 1811

Anguimorpha Fürbringer, 1900

Pan-Xenosaurus Smith and Gauthier, 2013

Remarks: The clade name Pan-Xenosaurus Smith and Gauthier, 2013 is a stem-based name intended to encompass the total clade of crown *Xenosaurus*. It is an approximate synonym of Xenosauridae Cope, 1886 sensu Conrad (2008), who similarly defined the name for a stem-based clade, except that Conrad (2008) did not include *Shinisaurus* Ahl, 1930, or *Heloderma* Wiegmann, 1829, in his definition. We prefer Pan-Xenosaurus here for two reasons. First, in the event that *Xenosaurus* is related to either of those taxa (although we are not aware of a molecular proposal for any such relationship), then additional extant taxa would be included in Xenosauridae. Second, the *pan-* convention promotes mutual comprehension amongst diverse taxonomists.

***Blutwurstia*,** new genus

This nomenclatural act has been registered in ZooBank, urn:lsid:zoobank.org:act:B9B42807-73AE-4743-9C21-9CBF6E79F717.

Type species: *Blutwurstia oliviae*, sp. nov.

Diagnosis: As for type and only known species.

Etymology: *Blutwurst*, German for (f.) "blood sausage," in reference to the coloration, tendency to gather or "link up" in groups, and habitus of its close modern relative, *Xenosaurus*.

Blutwurstia oliviae, new species

Figures 2–6

This nomenclatural act has been registered in ZooBank, urn:lsid:zoobank.org:act:261DB1A7-F9CB-4FE2-BC86-58B3DBA2B0EE

Holotype: USNM PAL 768729 (nearly complete left maxilla, left palpebral, left jugal, postdentary portion of left mandible, dorsal vertebra, presumably from a single individual).

Horizon and locality: 8abc Limestone, lower Eocene Willwood Formation, Wyoming.

Distribution: Known only from type locality.

Etymology: The made-up word "oliviae" is considered a noun in apposition (ICZN Article 31). Any similarity to the given name of O. Rieppel, whose contributions to our understanding of anguimorph lizards rank scarcely less than his contributions to philosophy of systematics, is purely coincidental. Such an honor might be seen as unctuous, olivaria (Latin, "of olives, olive oil").

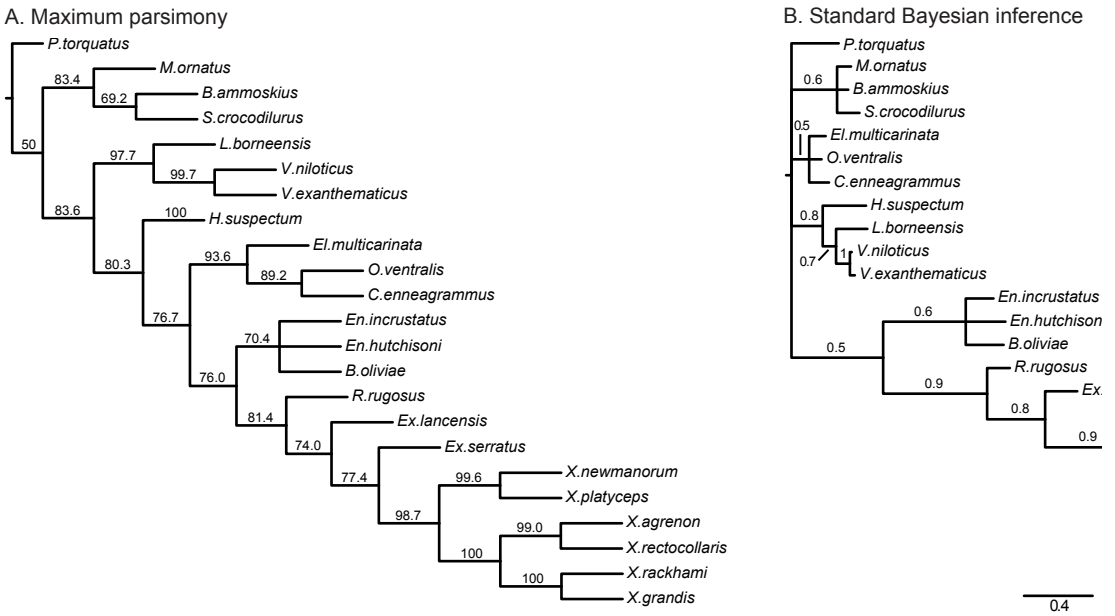

FIG. 8. Phylogenetic relationships of USNM PAL 768729 based on four methods (*above and opposite page*). **A**, Maximum parsimony with enforced molecular constraint. Numbers above branches are bootstrap support based on 1000 replications. Results with no constraint have identical topology with respect to Pan-Xenosaurus. **B**, Standard Bayesian inference. Numbers above branches are posterior probabilities. **C**, Fossilized birth-death

Diagnosis: Anguimorph lizard with trenchant, unicuspid, unstriated teeth lacking plicidentine. Shares with *Xenosaurus* (and other pan-xenosaurs, in which they are known) the following apomorphies: posterior portion of nasal facet of maxilla folded towards the vertical; palpebral shaped like equilateral triangle with short, blunt posterolateral process; foramen in jugal adductor surface; and dorsal vertebrae with very short neural spine and depressed centrum. Primitive with respect to *Restes*, *Exostinus* spp., and *Xenosaurus* in the following characters: teeth unicuspid, anterior end of lacrimal recess of maxilla more anterior, maxilla supradental thickening weak, and palpebral medial margin without S-curve. Shares with *Entomophontes* spp. the following apomorphies: increased length and reduced height of the facial process of the maxilla, increase in tooth diameter posteriorly in tooth row, and strong mesial and distal carinae on cheek teeth. Autapomorphies are its small size (SVL about 5 cm) and poor development of the osteodermal crust on facial process of the maxilla in ontogenetically advanced individuals.

Comments: While monophyly of *Entomophontes* with respect to *Blutwurstia* is neither supported nor rejected by our phylogenetic analyses, the two differ in a significant character not covered by the data matrix, namely the presence of a thick osteodermal crust (on the maxilla, at least; the frontal and parietal being unknown in *B. oliviae* and *E. hutchisoni*). As more of *B. oliviae* and *Entomophontes* spp. are discovered, it may become clear that recognition of *Blutwurstia* renders *Entomophontes* paraphyletic, in which case the former should be synonymized.

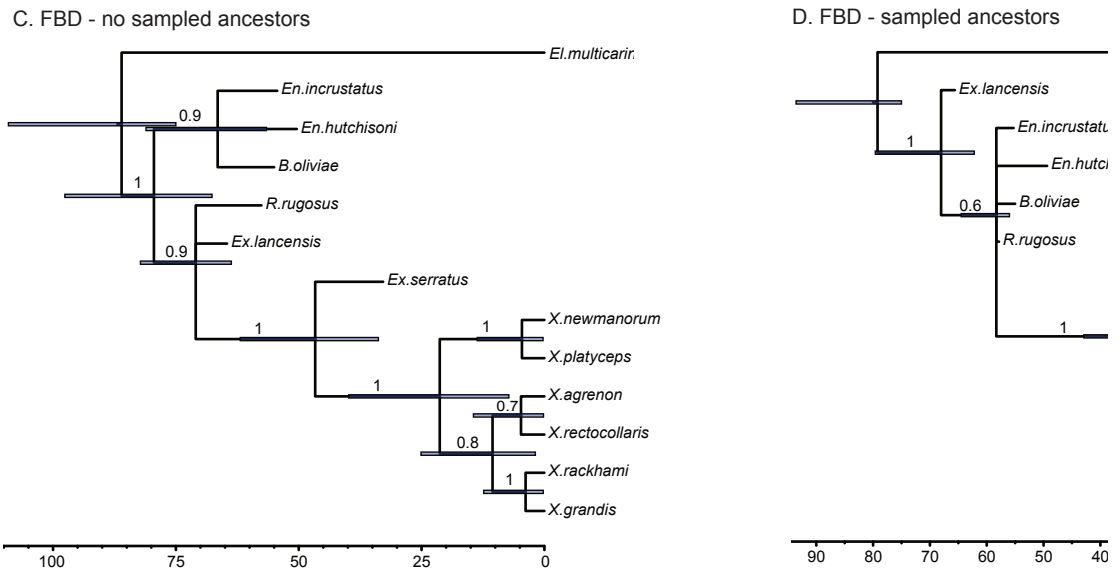

without sampled ancestors. Numbers above branches are posterior probabilities and horizontal bars are 95% confidence intervals on divergence time (lower axis, in Ma). **D,** Fossilized birth-death with sampled ancestors. Numbers above branches are posterior probabilities and horizontal bars are 95% confidence intervals on divergence time (lower axis, in Ma).

DISCUSSION

Taxonomy and Relationships

Gao and Fox (1996) challenged the previous contention (Estes, 1964) that *Exostinus lancensis* has incipiently bicuspid teeth, arguing that any such appearance might result from breakage of the mesial carina of the posterior teeth. Gilmore (1928) did not attribute incipient secondary cusps to this species, nor did Sahni (1972). Examination of the holotype (USNM PAL 10689) supports Estes' (1964) view in the sense that tiny accessory cusps are in fact developed on posterior cheek teeth and are not attributable to breakage (see also Bhullar, 2011). However, these accessory cusps differ from those seen in *Restes* and *Xenosaurus*, which are larger and separated by a moderately strong apicobasal groove; this groove is nearly absent in *Ex. lancensis*. Such an accessory cusp, even incipient, is clearly lacking in *Entomophontes* spp. and *Blutwurstia oliviae*.

The teeth of an unnamed xenosaurid described by Gao and Fox (1996: fig. 27H–J) from the Milk River Formation are flared in a manner similar to those of *Entomophontes* and *Blutwurstia oliviae* in having trenchant teeth with sharp mesial and distal blades. In light of the more recent descriptions of *Entomophontes* and *B. oliviae*, further study of those specimens, in particular the undescribed premaxilla referred to it by the same authors, is desirable. It seems possible that the unnamed species of Gao and Fox (1996) represents part of the same basal clade of Pan-Xenosaurus. If so, the Aquilan (early Campanian, 84–79 Ma) age of the Milk River

record would suggest that the divergence of this clade is in the earlier part of the range computed by our cal3 time-scaling (about 95–70 Ma) and FBD-noSA (96–68 Ma) analyses, and that the divergence of *Entomophontes* and *Blutwurstia* from other pan-xenosaurs (65–56 Ma) computed by our FBD-SA analysis is much too young.

The form of the teeth, with slightly flaring shafts at mid-height, is a potential synapomorphy of *Entomophontes* and *Blutwurstia oliviae*, and other potential synapomorphies were listed above. However, the osteodermal crust on the maxilla of specimens of the latter (like on the other cranial bones known from *En. incrustatus*) is much better developed in terms of extent and thickness (Smith and Gauthier, 2013). While similar differences in osteoderm development and ornamentation are documented between juvenile and adult representatives of some extant species, such as the anguid *Elgaria multicarinata* (Bhullar, 2012), terminal fusion of the scapula and coracoid suggests that the holotype of *B. oliviae* was ontogenetically advanced (see above). Reduction in body size in the anguid lizard *Anniella pulchra* is associated with reduced osteodermal ossification, a phenomenon attributed to paedomorphosis (Bhullar and Bell, 2008). It is possible that paedomorphosis in *B. oliviae* is responsible for the lesser ossification of the dermis overlying the cranial bones.

Ghost Lineages, Pseudoextinction, and the Fossilized Birth-Death Model

It has long been recognized that hypotheses of phylogenetic relationships can be incorporated into studies of past diversity, including diversity during mass extinction events (Norell, 1992; Archibald, 1993; Smith, 1994). In the most basic form, tree topology can imply the existence of "ghost lineages" that are unrecorded as fossils. On the other hand, it has also been recognized that ancestral-descendant relationships may play a significant role in the interpretation of extinction and origination rates in the fossil record (Archibald, 1993; 1994). In particular, if one morphospecies becomes so transformed that it is recognized as a new taxonomic species, then the "extinction" of the ancestor is not a true evolutionary event but rather "pseudoextinction." Archibald (1993) distinguished several models of speciation (different kinds of cladogenesis and anagenesis) and studied their implications for cladistic results. Modern models still distinguish between anagenesis, which does not add to diversity, and cladogenesis, especially budding, which does add to species diversity (e.g., Bapst, 2013; Bapst et al., 2016).

As calculated by Tracer v1.6.0, the proportion of fossils inferred to be ancestors in our analysis had a median of 0.33, that is, two of six fossil species (mean: 0.39, 95% credibility interval 0.17–0.83). From the consensus tree, the two species with the shortest branch lengths are *Ex. lancensis* (median branch length = 0, mean branch length = 0.053, 95% credibility interval = 0.0–0.37) and *R. rugosus* (median branch length = 0, mean branch length = 0.35, 95% credibility interval = 0.0–1.57). These two species are the best candidates for direct ancestors according to this model, raising the possibility that the two ghost lineages implied under maximum parsimony are too long (depending on the extent to which the descendant arose before the nominal extinction of the ancestor).

A literal reading of the fossil record (fig. 9A) shows that pan-xenosaur species diversity peaked (with a maximum of two) species in the early Eocene. There was a single known species extant at the K-Pg boundary, *Exostinus lancensis*, and it survived. A basic time-scaled phylogeny (not shown), however, based on the MP tree, shows that diversity was higher in the Late Cretaceous and Paleocene. This arises because the phylogenetic hypothesis implies that three more lineages first known in the Paleogene extended back into the Cretaceous: the clade *Entomophontes* spp. + *B. oliviae* as well as *R. rugosus* and more crownward Pan-Xenosaurus. Similarly, the three-rate calibrated (cal3) phylogenies also imply a shift of the peak of pan-xenosaur diversity to the latest Cretaceous and Paleocene (fig. 9B), with a median diversity of 4 species at the K-Pg boundary. The FBD-noSA trees similarly show an early diversity peak that encompasses the K-Pg boundary (fig. 9C); a median diversity of 4 lineages (2.5% and 97.5% quantiles: 2–6). This count is reduced for FBD-SA trees to a median of 3 (fig. 9D) in part because some lineages are ancestral to others. Furthermore, both the cal3 and FBD-noSA results suggest divergence times that occurred earlier than the divergences implied by basic time-scaling. The analysis using the TK02 clock model (results not shown) would produce results closer to the FBD-SA analysis.

It has been considered that phylogenetic trees will tend only to increase past taxic diversity, because they only extend lineages back in time (Wagner, 2000). For this reason, the backward temporal shift in the known peak of pan-xenosaur diversity is not very surprising. That this peak now embraces the Cretaceous-Paleogene boundary is of greater interest.

The nadir in species diversity in the late Eocene-Miocene could be explained as an artifact of inadequate sampling. It has been widely recognized (e.g., Estes, 1970; Gauthier, 1982) that taxa of tropical aspect had a greater latitudinal extent in the Eocene, when global climate was warmer and more equitable. Smith (2006, 2009) promulgated a biogeographic model in which taxa adapted to megathermal climates responded to global cooling after the Eocene by retreat or restriction toward the geographic tropics. Although we recognize that one pan-xenosaur species, *Exostinus serratus*, is known from the early Oligocene, if this clade behaved similarly, then much of its later Cenozoic evolution might be found in the southern United States and Mexico, from which few small reptile fossils have been described.

Paleoecology and K-Pg Survivorship in Pan-Xenosaurus

The low neural spine of the dorsal vertebrae in *B. oliviae* was noted above as an apomorphy suggesting a relationship with *Xenosaurus*. It is also a feature of ecomorphologic interest, suggesting a depressed body form or habitus. Dorsal vertebrae are unknown from *Entomophontes*, but a referred premaxilla (Smith and Gauthier, 2013: fig. 24A, B) has a nasal process projecting posterodorsally at a relatively low angle to the horizontal. While a precise estimate of the angle is difficult because the bones are disarticulated, the angle is lower than for other cryptozoic terrestrial lizards like *Diploglossus* (e.g., Bochaton et al., 2016). Furthermore, the facial process of the maxilla is also lower in *Entomophontes incrustatus* (Smith and Gauthier, 2013: fig. 24D), as it is in *En. hutchisoni* (Smith and Gauthier, 2013: fig. 26A) and *B. oliviae* (see Diagnosis

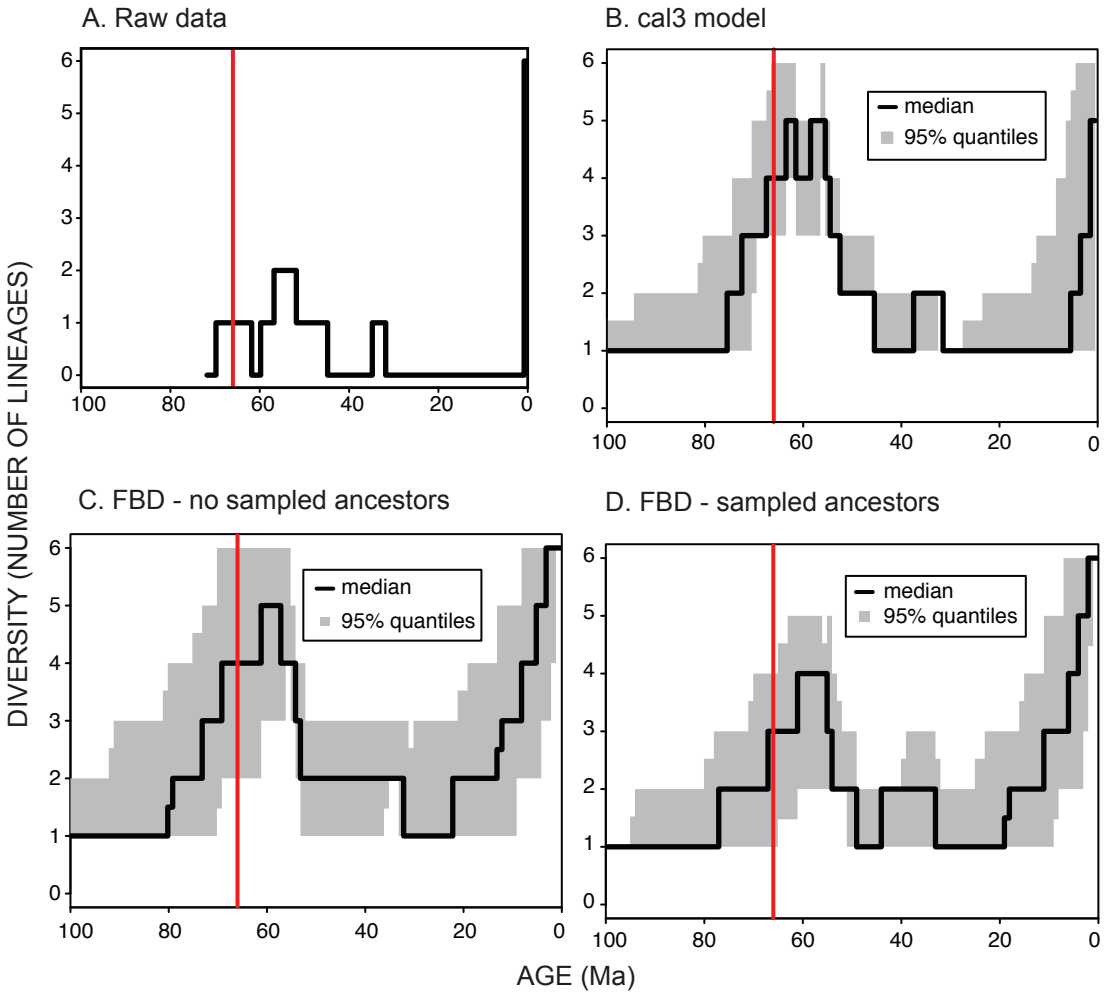

FIG. 9. Evolution of species diversity in Pan-Xenosaurus based on various models. Vertical red lines mark the K-Pg boundary. **A**, Raw species diversity calculated from ranges of known fossil species and no phylogenetic considerations. The peak of two species is in the early Eocene. **B**, Lineage-through-time plot based on cal3 model of Bapst (2013). The first peak is much higher and encompasses the Cretaceous–Paleogene boundary. **C**, Lineage-through-time plot based on 100 tree samples from the fossilized birth-death (FBD) analysis without sampled ancestors, showing similar peaks. **D**, Lineage-through-time plot based on 100 tree samples from the FBD analysis with sampled ancestors, showing similar peaks.

above). The generally short nasal process in *Xenosaurus* makes comparison with extant species difficult (see Bhullar, 2011: figs. 9, 10). These features of *Entomophontes* also point to a depressed body form, or at least a flattened skull profile. Together, they suggest that members of even the basal-most clade of Pan-Xenosaurus may have been crevice-dwellers—and parsimony optimization implies that occupation of this microhabitat is primitive for Pan-Xenosaurus at least as far rootward as that clade.

Another feature of ecological interest is size. Members of the basal clade were around 100 mm SVL or less (see above), and similar values obtain for other members of Pan-Xenosaurus.

Small lizards tend to be insectivorous rather than carnivorous or herbivorous (Pough, 1973), and the dentition of known members of Pan-Xenosaurus shows no adaptations for herbivory.

These features might have been particularly useful to pan-xenosaurs across the K-Pg boundary because they protected the animals from short- and medium-term consequences of the K-Pg bolide impact. A proposed consequence of the impact is a thermal pulse resulting from the transformation of kinetic energy into heat upon the reentry into the atmosphere of ejecta (Robertson et al., 2004; Schulte et al., 2010). The heat may not have been sufficient to cause woody biomass to ignite, especially wet woody biomass, but it would have a major deleterious influence on nonwoody vegetation. It is potentially related to the so-called fern spike, which has been documented in different regions of the globe and may indicate a pioneer vegetation (Vajda et al., 2001; Schulte et al., 2010). A further consequence of the impact may have been a severe restriction of primary productivity via atmospheric dust and aerosols, although productivity may have recovered within a time scale of decades (Sepúlveda et al., 2009).

We suggest that the higher species survivorship of pan-xenosaurs than other squamate clades is related to their crevice-dwelling habits, facilitated by small size (Longrich et al. 2012). Crevice-dwelling habits could have provided shelter from the initial thermal pulse, while insectivory made them less reliant on photosynthetic energy pathways. Similarly, aquatic vertebrates, except for elasmobranchs, are well documented to have a much higher survivorship across the K-Pg boundary (Archibald and Bryant, 1990; Fastovsky and Sheehan, 2005), possibly because the high heat capacity of water protected them from the thermal pulse, while their food chains were less dependent on photosynthesis (Sheehan and Hansen, 1986; Robertson et al., 2004).

CONCLUSIONS

The Cretaceous–Paleogene (K-Pg) boundary is marked by the impact of a bolide, thought to have resulted in large-scale destruction of terrestrial environments, particularly in North America (Schulte et al., 2010: and references therein). Large-scale extinction in the marine realm (MacLeod et al., 1997) was accompanied by the final extinction of nonavian dinosaurs on land and perhaps pterosaurs as well. Similarly, a substantial extinction of squamate reptiles in North America (Longrich et al., 2012) occurred, although it is possible that similar phylogenetic diversity studies of other squamate clades might reduce the apparent level of extinction. Regardless, the coincidence of these two events—bolide impact and mass extinction—together with plausible kill mechanisms has convinced many that the former caused the latter (Brusatte et al., 2015). Other causes or contributors to the extinction are still being evaluated (Archibald et al., 2010).

Pan-Xenosaurus is particularly interesting in this context because it was present in North America at proximal (<1000 km) to intermediate (1000–5000 km) distance to Chicxulub at the time of the impact and has a relict distribution today in Mexico and Central America. Species diversity in *Xenosaurus* is apparently higher than previously thought—the most recent estimates put it at 18—but the species tend to be microendemic, in keeping with their secretive habits and stenotopic distribution, which may limit mobility and gene flow.

New methods such as cal3 and the fossilized birth-death model are now available that directly incorporate stratigraphic data and allow study of diversity patterns in a phylogenetic context that also takes account of ancestral-descendant relations (e.g., Parins-Fukuchi, 2021). These methods can extend ghost lineages beyond the point at which the lineage or its sister is first documented in the fossil record, and to some extent they may therefore help to recover even lineages that are evolving independently even before they have acquired new apomorphic features that allow them to be recognized. And in explicitly allowing for the possibility of ancestral forms, they provide a probabilistic means to recognize pseudoextinction.

Results from our phylogenetic analyses suggest that 3–4 lineages of Pan-Xenosaurus were present in the latest Cretaceous and all survived the K-Pg boundary. The survival of such lineages is even more remarkable considering their apparent proximity to the bolide impact. Two members of the basalmost clade of Pan-Xenosaurus, namely *Blutwurstia oliviae* and *Entomophontes incrustatus*, possess morphological features consistent with a depressed habitus, which suggests they were already crevice-dwellers, like extant *Xenosaurus*. If so, this might have contributed to their survival across an interval of widespread habitat destruction. Nevertheless, given that so few elements are known in common between *Blutwurstia* and *Entomophontes*, and evidence for a crevice-dwelling habits is limited, more complete specimens will be necessary to test these conclusions more thoroughly.

ACKNOWLEDGMENTS

Peter Houde (New Mexico State University) found and prepared the fossils of *Blutwurstia oliviae*, and Amanda Millhouse (USNM) helped with cataloging the specimen. Bob Rainey (University of Texas at Austin) also helped with preparation. Matt Carrano (USNM), Kenney Krysko (UF), Stephen Rogers (CM), and Eric Scott (San Bernardino County Museum) kindly provided access to specimens in their care. We are indebted to Jacques Gauthier for profitable discussions. Arnau Bolet and Keqin Gao thoroughly read the manuscript and we are grateful for their attentive criticisms, which improved the paper. Financial support came from the Texas Memorial Museum at the University of Texas at Austin and the Senckenberg Research Institute.

REFERENCES

Alvarez, L.W., W. Alvarez, F. Asaro, and H.V. Michel. 1980. Extraterrestrial cause for the Cretaceous-Tertiary extinction. Science 208: 1095–1108.

Archibald, J.D. 1993. The importance of phylogenetic analysis for the assessment of species turnover – a case history of Paleocene mammals in North America. Paleobiology 19 (1): 1–27.

Archibald, J.D. 1994. Metataxon concepts and assessing possible ancestry using phylogenetic systematics. Systematic Biology 43 (1): 27–40.

Archibald, J.D., and L.J. Bryant. 1990. Differential Cretaceous/Tertiary extinctions of nonmarine vertebrates; evidence from northeastern Montana. Geological Society of America Special Paper 247: 549–562.

Archibald, J.D., et al. 2010. Cretaceous extinctions: multiple causes. Science 328: 973.

Bapst, D.W. 2012. Paleotree: an R package for paleontological and phylogenetic analyses of evolution. Methods in Ecology and Evolution 3 (5): 803–807.

Bapst, D.W. 2013. A stochastic rate-calibrated method for time-scaling phylogenies of fossil taxa. Methods in Ecology and Evolution 4 (8): 724–733.

Bapst, D.W., A.M. Wright, N.J. Matzke, and G.T. Lloyd. 2016. Topology, divergence dates, and macroevolutionary inferences vary between different tip-dating approaches applied to fossil theropods (Dinosauria). Biology Letters 12 (7): 20160237.

Bartels, W.S. 1987. Fossil reptile assemblages and depositional environments of selected early Tertiary vertebrate bone concentrations, Bighorn Basin, Wyoming. Ph.D. dissertation, Department of Geology, University of Michigan, Ann Arbor, Michigan.

Beard, K.C., and P. Houde. 1989. An unusual assemblage of diminutive plesiadapiformes (Mammalia, ?Primates) from the early Eocene of the Clarks Fork Basin, Wyoming. Journal of Vertebrate Paleontology 9 (4): 388–399.

Bell, M.A., and G.T. Lloyd. 2015. Strap: an R package for plotting phylogenies against stratigraphy and assessing their stratigraphic congruence. Palaeontology 58 (2): 379–389.

Bhullar, B.-A.S. 2010. Cranial osteology of *Exostinus serratus* (Squamata: Anguimorpha), fossil sister taxon to the enigmatic clade *Xenosaurus*. Zoological Journal of the Linnean Society 159: 921–953.

Bhullar, B.-A.S. 2011. The power and utility of morphological characters in systematics: a fully resolved phylogeny of *Xenosaurus* and its fossil relatives (Squamata: Anguimorpha). Bulletin of the Museum of Comparative Zoology 160 (3): 65–181.

Bhullar, B.-A. S. 2012. A phylogenetic approach to ontogeny and heterochrony in the fossil record: cranial evolution and development in anguimorphan lizards (Reptilia: Squamata). Journal of Experimental Zoology B 318: 521–530.

Bhullar, B.-A.S., and C.J. Bell. 2008. Osteoderms of the legless lizard *Anniella* (Squamata: Anguidae) and their relevance for considerations of miniaturization. Copeia 2008 (4): 785–793.

Bloch, J.I., and G.J. Bowen. 2001. Paleocene-Eocene microvertebrates in freshwater limestones of the Willwood Formation, Clarks Fork Basin, Wyoming. *In* G.F. Gunnell (editor), Eocene biodiversity: unusual occurrences and rarely sampled habitats: 96–129. New York: Kluwer Academic.

Bloch, J.I., and D.M. Boyer. 2001. Taphonomy of small mammals in freshwater limestones from the Paleocene of the Clarks Fork Basin. *In* P.D. Gingerich (editor), Paleocene-Eocene stratigraphy and biotic change in the Bighorn and Clarks Fork basins, Wyoming: 185–198. Ann Arbor, MI: Museum of Paleontology, University of Michigan.

Bochaton, C., R. Boistel, F. Casagrande, S. Grouard, and S. Bailon. 2016. A fossil *Diploglossus* (Squamata, Anguidae) lizard from Basse-Terre and Grande-Terre islands (Guadeloupe, French West Indies). Scientific Reports 6: 1–12.

Bowen, G.J., and J.I. Bloch. 2002. Petrography and geochemistry of floodplain limestones from the Clarks Fork Basin, Wyoming, USA: Carbonate deposition and fossil accumulation on a Paleocene-Eocene floodplain. Journal of Sedimentary Research 72 (1): 46–58.

Brocklehurst, N., C.F. Kammerer, and J. Fröbisch. 2013. The early evolution of synapsids, and the influence of sampling on their fossil record. Paleobiology 39 (3): 470–490.

Brusatte, S.L., et al. 2015. The extinction of the dinosaurs. Biological Reviews 90 (2): 628–642.

Bryant, L.J. 1989. Non-dinosaurian lower vertebrates across the Cretaceous-Tertiary boundary in northeastern Montana. University of California Publications in Geological Sciences 134: 1–107.

Burbrink, F.T., et al. 2020. Interrogating genomic-scale data for squamata (lizards, snakes, and amphisbaenians) shows no support for key traditional morphological relationships. Systematic Biology 69: 502–520.

Caldwell, M.W. 2003. Holotype snout elements of *Saniwa ensidens* reassigned to cf. *Restes* sp. Indet. (Xenosauridae). Journal of Paleontology 77 (2): 393–396.

Čerňanský, A., K.T. Smith, and J. Klembara. 2014. Variation in the position of the jugal medial ridge among lizards (Reptilia: Squamata): Its functional and taxonomic significance. Anatomical Record 297: 2262–2272.

Čerňanský, A., et al. 2019. Vertebral comparative anatomy and morphological differences in anguine lizards with a special reference to *Pseudopus apodus*. Anatomical Record 302: 232–257.

Cifelli, R.L., J.J. Eberle, D.L. Lofgren, J.A. Lillegraven, and W.A. Clemens. 2004. Mammalian biochronology of the latest Cretaceous. *In* M.O. Woodburne (editor), Late Cretaceous and Cenozoic mammals of North America: biostratigraphy and geochronology: 21–42. New York: Columbia University Press.

Conrad, J.L. 2008. Phylogeny and systematics of Squamata (Reptilia) based on morphology. Bulletin of the American Museum of Natural History 310: 1–182.

Conrad, J.L., J.C. Ast, S. Montanari, and M.A. Norell. 2011. A combined evidence phylogenetic analysis of Anguimorpha (Reptilia: Squamata). Cladistics 27: 230–277.

Cope, E.D. 1873. Synopsis of new vertebrata from the Tertiary of Colorado, obtained during the summer of 1873. Annual Report of the United States Geological Survey of the Territories 7: 3–19.

Cope, E.D. 1892. The osteology of the Lacertilia. Proceedings of the American Philosophical Society 30: 185–221.

Dupuis, C., et al. 2003. The Dababiya Quarry section: lithostratigraphy, clay mineralogy, geochemistry and paleontology. Micropaleontology 49 (Suppl. 1): 41–59.

Estes, R. 1964. Fossil vertebrates from the Late Cretaceous Lance Formation, eastern Wyoming. University of California Publications in Geological Sciences 49: 1–187.

Estes, R. 1970. Origin of the Recent North American lower vertebrate fauna: an inquiry into the fossil record. Forma et Functio 3: 139–163.

Estes, R. 1976. Middle Paleocene lower vertebrates from the Tongue River Formation, southeastern Montana. Journal of Paleontology 50 (3): 500–520.

Estes, R. 1983. Sauria Terrestria, Amphisbaenia (Handbuch der Paläoherpetologie, v. 10a), Stuttgart: Gustav Fischer Verlag.

Fastovsky, D.E., and P.M. Sheehan. 2005. The extinction of the dinosaurs in North America. GSA Today 15 (3): 4–10.

Flynn, J.J., and L. Tauxe. 1998. Magnetostratigraphy of upper Paleocene–lower Eocene marine and terrestrial sequences. *In* M.-P. Aubry, W.A. Berggren, and S.G. Lucas (editors), Late Paleocene–Early Eocene biotic and climatic events in the marine and terrestrial Records: 67–90. New York: Columbia University Press.

Fry, B.G., et al. 2006. Early evolution of the venom system in lizards and snakes. Nature 439: 584–588.

Gao, K., and R.C. Fox. 1996. Taxonomy and evolution of Late Cretaceous lizards (Reptilia: Squamata) from western Canada. Bulletin of the Carnegie Museum of Natural History 33: 1–107.

Gauthier, J., M. Kearney, J.A. Maisano, O. Rieppel, and A. Behlke. 2012. Assembling the squamate tree of life: perspectives from the phenotype and the fossil record. Bulletin of the Peabody Museum of Natural History 53: 3–308.

Gauthier, J.A. 1982. Fossil xenosaurid and anguid lizards from the early Eocene Wasatch Formation, southeast Wyoming, and a revision of the Anguioidea. Contributions to Geology, University of Wyoming 21 (1): 7–54.

Gilmore, C.W. 1928. Fossil lizards of North America. Memoirs of the National Academy of Sciences 22: 1–201.

Gilmore, C.W. 1942. Paleocene faunas of the Polecat Bench Formation, Park County, Wyoming. Part II. Lizards. Proceedings of the American Philosophical Society 85 (2): 159–167.

Gingerich, P.D. 2001. Biostratigraphy of the continental Paleocene-Eocene boundary interval on Polecat Bench in the northern Bighorn Basin. University of Michigan Papers on Paleontology 33: 33–71.

Haas, G. 1960. On the Trigeminus Muscles of the Lizards *Xenosaurus grandis* and *Shinisaurus crocodilurus*. American Museum Novitates 2017: 1–54.

Hedges, S.B., and N. Vidal. 2009. Lizards, snakes, and amphisbaenians (Squamata). *In* S.B. Hedges and S. Kumar (editors), The timetree of life: 383–389. Oxford: Oxford University Press.

Klembara, J., and A. Čerňanský. 2020. Revision of the cranial anatomy of *Ophisaurus acuminatus* Jörg, 1965 (Anguimorpha, Anguidae) from the late Miocene of Germany. Geodiversitas 42: 539–557.

Lemos-Espinal, J., G.R. Smith, and G. Woolrich-Piña. 2012. La familia Xenosauridae en México/the family Xenosauridae in Mexico, Rodeo, New Mexico: ECO Herpetological Publishing and Distribution.

Lepage, T., D. Bryant, H. Philippe, and N. Lartillot. 2007. A general comparison of relaxed molecular clock models. Molecular Biology and Evolution 24: 2669–2680.

Lewis, P.O. 2001. A likelihood approach to estimating phylogeny from discrete morphological character data. Systematic Biology 50 (6): 913–925.

Longrich, N.R., B.-A.S. Bhullar, and J.A. Gauthier. 2012. Mass extinction of lizards and snakes at the cretaceous-paleogene boundary. Proceedings of the National Academy of Sciences of the United States of America 109: 21396–21401.

MacLeod, N., et al. 1997. The Cretaceous-Tertiary biotic transition. Journal of the Geological Society 154: 265–292.

Maisano, J.A. 2002. Terminal fusions of skeletal elements as indicators of maturity in squamates. Journal of Vertebrate Paleontology 2002 (22): 2.

Matzke, N.J., and A.J. Wright. 2016. Inferring node dates from tip dates in fossil Canidae: the importance of tree priors. Biology Letters 12 (8): 20160328.

McCarroll, S.M., J.J. Flynn, and W.D. Turnbull. 1996. Biostratigraphy and magnetostratigraphy of the Bridgerian-Uintan Washakie Formation, Washakie Basin, Wyoming. *In* D.R. Prothero and R.J. Emry (editors), The terrestrial Eocene-Oligocene transition in North America: 25–39. New York: Cambridge University Press.

Nieto-Montes de Oca, A., et al. 2017. Phylogenomics and species delimitation in the knob-scaled lizards of the genus *Xenosaurus* (Squamata: Xenosauridae) using ddRADseq data reveal a substantial underestimation of diversity. Molecular Phylogenetics and Evolution 106: 241–253.

Norell, M.A. 1992. Taxic origin and temporal diversity: the effect of phylogeny. *In* M.J. Novacek and Q.D. Wheeler (editors), Extinction and Phylogeny: 89–118. New York: Columbia University Press.

Norell, M.A., and K. Gao. 1997. Braincase and phylogenetic relationships of *Estesia mongoliensis* from the Late Cretaceous of the Gobi Desert and the recognition of a new clade of lizards. American Museum Novitates 3211: 1–25.

Norell, M.A., M.C. McKenna, and M.J. Novacek. 1992. *Estesia mongoliensis*, a new fossil varanoid from the Late Cretaceous Barun Goyot Formation of Mongolia. American Museum Novitates 3045: 1–24.

Nydam, R.L. 2000. A new taxon of helodermatid-like lizard from the Albian-Cenomanian of Utah. Journal of Vertebrate Paleontology 20 (2): 285–294.

Nydam, R.L. 2013. Squamates from the Jurassic and Cretaceous of North America. Palaeobiodiversity and Palaeoenvironments 93 (4): 535–565.

Oelrich, T.M. 1956. The anatomy of the head of *Ctenosaura pectinata* (Iguanidae). Miscellaneous Publications, Museum of Zoology, University of Michigan 94: 1–122.

Parins-Fukuchi, C. 2021. Morphological and phylogeographic evidence for budding speciation: an example in hominins. Biology Letters 17: 20200754.

Pough, F.H. 1973. Lizard energetics and diet. Ecology 54 (4): 837–844.

Prothero, D.R., and R.J. Emry. 2004. The Chadronian, Orellan, and Whitneyan North American land mammal ages. *In* M.O. Woodburne (editor), Late Cretaceous and Cenozoic mammals of North America: biostratigraphy and geochronology: 156–168. New York: Columbia University Press.

Prothero, D.R., and C.C. Swisher. 1992. Magnetostratigraphy and geochronology of the terrestrial Eocene-Oligocene transition in North America. *In* D.R. Prothero and W.A. Berggren (editors), Eocene-Oligocene biotic and climatic evolution: 46–73. Princeton, NJ: Princeton University Press.

Pyron, R.A., F.T. Burbrink, and J.J. Wiens. 2013. A phylogeny and revised classification of squamata, including 4161 species of lizards and snakes. BMC Evolutionary Biology 13: 93.

Reeder, T.W., et al. 2015. Integrated analyses resolve conflicts over squamate reptile phylogeny and reveal unexpected placements for fossil taxa. PLoS One 10 (3): e0118199.

Revell, L.J. 2012. Phytools: an R package for phylogenetic comparative biology (and other things). Methods in Ecology and Evolution 3: 217–223.

Robertson, D.S., M.C. McKenna, O.B. Toon, S. Hope, and J.A. Lillegraven. 2004. Survival in the first hours of the Cenozoic. Geological Society of America Bulletin 116 (5-6): 760–768.

Ronquist, F., et al. 2012. Mrbayes 3.2: Efficient Bayesian phylogenetic inference and model choice across a large model space. Systematic Biology 61 (3): 539–542.

Sahni, A. 1972. The vertebrate fauna of the Judith River Formation, Montana. Bulletin of the American Museum of Natural History 147 (6): 321–412.

Schulte, P., et al. 2010. The Chicxulub asteroid impact and mass extinction at the Cretaceous-Paleogene boundary. Science 327: 1214–1218.

Secord, R. 2008. The Tiffanian land-mammal age (middle and late Paleocene) in the northern Bighorn Basin, Wyoming. University of Michigan Papers on Paleontology 35: 1–192.

Secord, R., et al. 2006. Geochronology and mammalian biostratigraphy of middle and upper Paleocene continental strata, Bighorn Basin, Wyoming. American Journal of Science 306 (4): 211–245.

Sepúlveda, J., J.E. Wendler, R.E. Summons, and K.U. Hinrichs. 2009. Rapid resurgence of marine productivity after the Cretaceous-Paleogene mass extinction. Science 326: 129–132.

Sheehan, P.M., and T.A. Hansen. 1986. Detritus feeding as a buffer to extinction at the end of the Cretaceous. Geology 14: 868–870.

Simões, T., M.W. Caldwell, and S.E. Pierce. 2020. Sphenodontian phylogeny and the impact of model choice in Bayesian morphological clock estimates of divergence times and evolutionary rates. BMC Biology 18: 191.

Smith, A.B. 1994. Systematics and the fossil record: documenting evolutionary patterns. London: Blackwell.

Smith, K.T. 2001. Reassessing the *Lambdotherium* first appearance datum (Wasatchian, early Eocene) in the Bighorn Basin, Wyoming. PaleoBios 21 (2): 1–11.

Smith, K.T. 2006. A diverse new assemblage of late Eocene squamates (Reptilia) from the Chadron Formation of North Dakota, U.S.A. Palaeontologia Electronica 9.2.5A(2): 44 pp.

Smith, K.T. 2009. A new lizard assemblage from the earliest Eocene (zone Wa0) of the Bighorn Basin, Wyoming, USA: Biogeography during the warmest interval of the cenozoic. Journal of Systematic Palaeontology 7 (3): 299–358.

Smith, K.T. 2011. The long-term history of dispersal among lizards in the early Eocene: New evidence from a microvertebrate assemblage in the Bighorn Basin of Wyoming, USA. Palaeontology 54 (6): 1243–1270.

Smith, K.T., and J.A. Gauthier. 2013. Early Eocene lizards of the Wasatch Formation near Bitter Creek, Wyoming: diversity and paleoenvironment during an interval of global warming. Bulletin of the Peabody Museum of Natural History 54 (2): 135–230.

Smith, K.T., et al. 2021. A model of digestive tooth corrosion in lizards: experimental tests and taphonomic implications. Scientific Reports 11: 12877.

Stadler, T. 2010. Sampling-through-time in birth-death trees. Journal of Theoretical Biology 267: 396–404.

Sullivan, R.M. 1982. Fossil lizards from Swain Quarry "Fort Union Formation," middle Paleocene (Torrejonian), Carbon County, Wyoming. Journal of Paleontology 56 (4): 996–1010.

Thorne, J. L., and H. Kishino. 2005. Divergence time and evolutionary rate estimation with multilocus data. Systematic Biology 51 (5): 689–702.

Vajda, V., J.I. Raine, and C.J. Hollis. 2001. Indication of global deforestation at the Cretaceous-Tertiary boundary by New Zealand fern spike. Science 294: 1700–1702.

Vidal, N., et al. 2012. Molecular evidence for an asian origin of monitor lizards followed by Tertiary dispersals to Africa and Australasia. Biology Letters 8: 853–855.

Wagner, P.J. 2000. The quality of the fossil record and the accuracy of phylogenetic inferences about sampling and diversity. Systematic Biology 49 (1): 65–86.

Wing, S.L., T.M. Bown, and J.D. Obradovich. 1991. Early Eocene biotic and climatic change in interior western North America. Geology 19 (12): 1189–1192.

Woolrich-Piña, G., and G.R. Smith. 2012. A new species of *Xenosaurus* from the Sierra Madre Oriental, Mexico. Herpetologica 68 (4): 551–559.

Yans, J., et al. 2006. High-resolution carbon isotope stratigraphy and mammalian faunal change at the Paleocene-Eocene boundary in the Honeycombs area of the southern Bighorn Basin, Wyoming. American Journal of Science 306: 712–735.

Yi, H.-Y., and M.A. Norell. 2013. New materials of *Estesia mongoliensis* (Squamata: Anguimorpha) and the evolution of venom grooves in lizards. American Museum Novitates 3767: 1–31.

Zhang, C., T. Stadler, S. Klopfstein, T.A. Heath, and F. Ronquist. 2016. Total-evidence dating under the fossilized birth-death process. Systematic Biology 65 (2): 228–249.

Zheng, Y., and J.J. Wiens. 2016. Combining phylogenomic and supermatrix approaches, and a time-calibrated phylogeny for squamate reptiles (lizards and snakes) based on 52 genes and 4162 species. Molecular Phylogenetics and Evolution 94: 537–547.

APPENDIX

Measurements of Snout-Vent Length and Maxillary Tooth Height in Iguanid Lizards

Genus	Species	Specimen	SVL (mm)	Maxillary tooth height (mm)
Sceloporus	*clarkii*	UF 54914	89	1.55
Sceloporus	*formosus*	UF 62083	85	1.6
Sceloporus	*grammicus*	UF 60671	55	1.3
Sceloporus	*serrifer*	UF 54560	93	1.55
Leiocephalus	*inaguae*	UF 99247	79	1.6
Leiocephalus	*lunatus*	UF 66071	65	1.25
Leiocephalus	*personatus*	UF 99341	65	1.3
Microlophus	*occipitalis*	UF 99683	55	1.1
Tropidurus	*hispidus*	UF 61630	79	2
Tropidurus	*torquatus*	UF 99338	78	1.75
Plica	*umbra*	UF 43638	95	2.25
Uracentron	*azureum*	UF 66078	95	2.55
Gambelia	*wislizenii*	UF 54056	100	1.9
Dipsosaurus	*dorsalis*	UF 55334	110	1.75
Ctenosaura	*similis*	UF 67982	263	4.15
Laemanctus	*longipes*	UF 66061	110	2.35
Corytophanes	*hernandesii*	CM 57586	106	2.05
Anolis	*armouri*	UF 99504	60	1.45
Anolis	*acutus*	UF 62414	55	1.2
Anolis	*chlorocyanus*	UF 99949	65	1.4
Anolis	*cristatellus*	UF 99457	55	1.25
Anolis	*cybotes*	UF 99927	65	1.55
Anolis	*garmani*	UF 42404	125	2.25
Anolis	*grahami*	UF 99166	73	1.65
Anolis	*lividus*	UF 48327	61	1.5
Anolis	*olssoni*	UF 99681	41	0.75
Anolis	*ortonii*	UF 68185	71	1.4
Anolis	*ricordii*	UF 99672	169	3.6
Anolis	*sagrei*	UF 99521	55	1.25
Anolis	*scriptus*	UF 99541	42	0.9
Anolis	*smaragdinus*	UF 99381	49	0.9
Anolis	*wattsi*	UF 24019	46.5	1.2
Anolis	*whitemani*	UF 99686	64	1.3